Western Graduate&PostdoctoralStudies

Western University

Scholarship@Western

Electronic Thesis and Dissertation Repository

3-22-2019 2:45 PM

Investigation and Modeling of the Dip Coating for Dispersions with Near Wall Effects

Mahdieh Moghadasi
The University of Western Ontario

Supervisor
Hrymak Andrew
The University of Western Ontario

Follow this and additional works at: https://ir.lib.uwo.ca/etd

Part of the Complex Fluids Commons

Abstract

The key to controlling the quality of liquid dispersion coated films lies in the particle distribution in the flow field. The control of particle dispersion in the film can also empower the optimization of the process operation. Therefore, a numerical simulation of a solid-liquid suspension in the dip coating (free withdrawal) process using the finite element method for the fluid flow has been developed. The neutrally buoyant suspension is considered as a Newtonian fluid with a concentration-dependent viscosity.

A continuum constitutive equation is employed based on the diffusive flux model in two-dimensional flow. The main purpose of this study is used to assess the shear-induced migration phenomenon in free-surface of concentrated suspension and the effects of the coating bath walls near the substrate to explore the particle distribution in the flow field.

Other parameters studied include particle concentration, particle radius, and withdrawal speed. The simulation results show a highly nonuniform distribution of particles in the coating film and recirculation regions. The suspension flow model predicts regions of low and high particle concentration compared to the average concentration. Higher concentration region presents at the middle and outer part of the coating film, varied depending on the parameter. Lower concentration region presents at the moving substrate region. Certainly, the nonuniform shear flow and the shape of the interface induces particle migration in concentrated suspension in the dip coating process.

Keywords

Acknowledgments

This work is conducted under the guidance of my supervisor, Dr. Andrew Hrymak to whom I pay great gratitude and respect. I appreciate the time and guidance he has given to me. His supervision helped me in all the time of research and writing of this thesis.

Finally, I must express my very profound gratitude to my family for their support. I thank my siblings, for giving me the foundation and support to get to where I am. This accomplishment would not have been possible without them.

Table of Contents

List of Tables

List of Figures

List of Symbols

e_β	a unit vector in the coordinate directions
g	acceleration of gravity
Bo	Bond number
Ca	capillary number
L	characteristic length
V	component of suspension velocity in vertical direction
$\zeta_i(x)$	concentration basis function
Co	Courant number
p_i	denotes the pressure at node i
v_i	denotes the velocity at node i
$D_\varphi \ and \ D_\mu$	diffusion coefficients
l_c	Dimensionless thickness in dip coating process
l_f	Dimensionless thickness in dip coating process
P_{ex}	external applied pressure
T	fluid stress tensor
$\dot{\gamma}$	local shear rate
ρ_f	mass concentration of the fluid phase
ρ_s	mass concentration of the particle phase
R^m	momentum residual

f	Newton correction factor
φ	particle concentration
J_s	particle flux
a	particle radius
D	particle Stokes-Einstein diffusion coefficient
Pe	Péclet number
p	pressure
$\psi_i(x)$	pressure shape function
μ_f	pure fluid viscosity
μ_r	relative viscosity
Re	Reynolds number
$\xi_i(x)$	Shear rate basic function
St	Stokes number
U	substrate speed
H	surface Curvature
∇_s	surface divergence operator
σ	surface tension
v_s	surface velocity
h_e	the average size of the element
x	the horizontal coordinate of the physical domain

E	the magnitude of second invariant shear rate
φ_m	the maximum packing volume fraction of particles
L_∞	the norm of the residual
n	the unit normal vector to the free surface
μ	the viscosity of the liquid
ρ	Total density
U_t	transition speed
ϕ_i	velocity basis function
y	vertical coordinate of the physical domain
We	Weber number

Chapter 1

1 « Introduction»

Coating a substrate via a dip coating process, or free withdrawal coating, through a bath containing a suspension of concentrated particles is examined in this study. A general overview of fluid behavior in this process, and the determining forces, which play a crucial role during the withdrawal process is provided.

In particular, the effect of the presence of a near wall to the free surface in the dip coating process is elucidated by examining the particle distribution through a numerical modeling approach.

Dip coating is commonly used to deposit a thin and uniform layer of film on different geometries of substrates. The most outstanding characteristic of dip coating processes is its simplicity and cost-effective usage. Dip coating is sufficiently flexible to produce films on irregularly shaped items and can be employed with different types of fluids (Park and Homsy, 1984; Ryck and Quéré, 1996; Krechetnikov and Homsy, 2005; Krechetnikov and Homsy, 2006; Afanasiev et al., 2007).

1.1 « Background Information »

Dip coating applications vary in industrial manufacturing, and also have been the focus of academic studies where it is required to create a thin layer of coating. Process conditions to achieve a desirable coating thickness is strongly dependent on the nature of the coating fluid entrained into the final film.

The schematic withdrawal process is shown in Figure 1 for the substrate based on the classic Landau-Levich model (Landau. and Levich, 1942) (White and Tallmadge, 1966; Roy and Dutt, 1981).
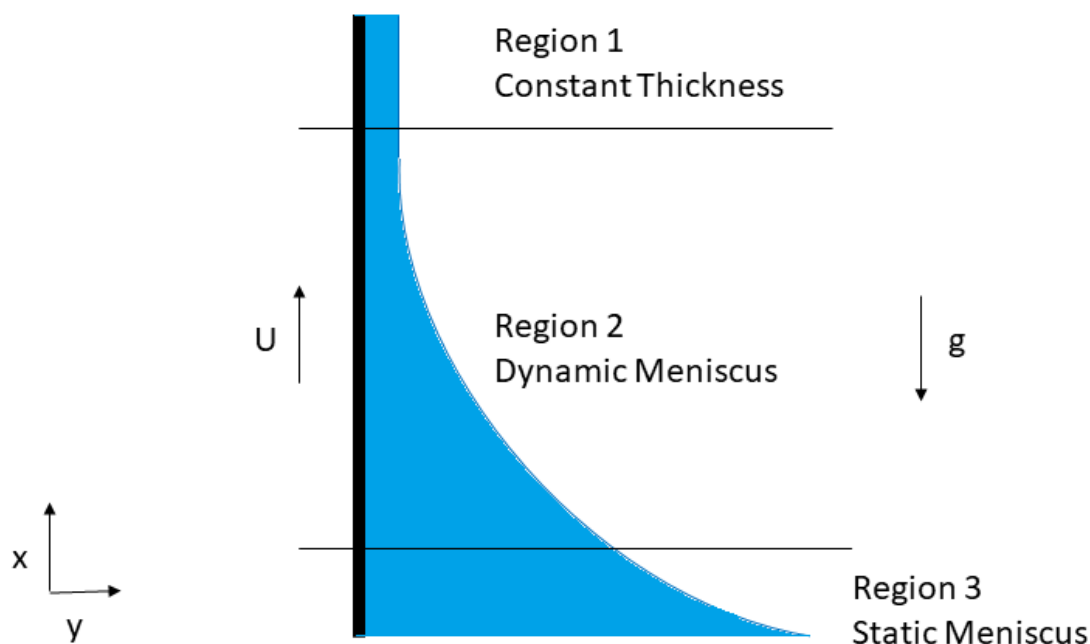
Figure 1: Three regions of withdrawal

There are several forces which play significant roles in the process of withdrawing the substrate from a liquid: surface tension, viscous force, inertia, and gravity.

There is a competition between these forces. The interplay between viscous forces and inertial forces defined by Reynolds number which is represented as the well-known equation, $Re = U.L.\rho /\mu$, where μ and ρ are the viscosity and density of the liquid respectively, L is a characteristic length. The capillary number state the relation between surface tension and viscous forces and calculated based on the following equation, $Ca = \mu.U/\sigma$, where σ is the surface tension. Ca is an important number in the dip coating process. The Stokes number ($St = g. L^2. \rho / \mu .U$) defines the relation between viscous and gravitational forces while the Bond number ($Bo = g. L^2. \rho/ \sigma$) is the relationship between surface tension and gravitational force (Sartor and Scriven, 1990)

One of the determinative factors that influence liquid film flow is the free surface morphology, which complicates the dip coating problem in the region near the point where the substrate leaves the liquid bath surface (Middleman, 1977).

At the free surface, the entrained liquid split into two viscous layers. In fact, the stagnation line is a dividing streamline between the two parts of the flow. As is shown in Figure 2 in shear flow region, close to the substrate, the fluid continues into the final film while in the recirculation flow region, gravity causes the fluid return to the bath so flow on both sides of this line either continue into the final film or return to the liquid bath. (Schunk et al., 1997; Colosqui et al., 2013)

Film-Entrainment Region

Stagnation Line

Static Meniscus Region
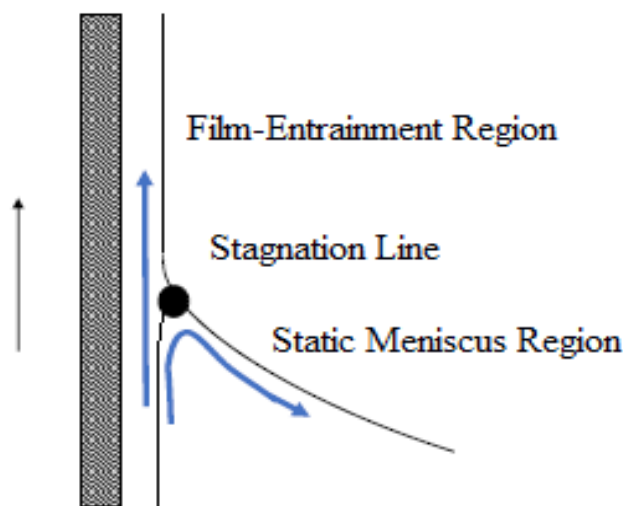
Figure 2: Dip coating schematic

At stagnation point, the fluid does not move, and velocity is zero. The streamlines separating the downward and upward moving layers are associated with the film thickness. Competition between the aforementioned forces determines the location of these streamlines and also the film thickness (Scriven, 1988; Brinker, 2013).

The approach for finding the film thickness can be calculated by solving Navier-Stokes and continuity equations using the following assumptions. Fluid is laminar, isothermal and incompressible, inertia is absent as well. The substrate is withdrawn vertically from a large bath containing Newtonian liquid at a constant speed.

The equations are expressed as follow:

$$\frac{\partial u}{\partial x} + \frac{\partial v}{\partial y} = 0 \tag{1}$$

$$\rho \left[u\frac{\partial u}{\partial x} + v\frac{\partial u}{\partial y} \right] = \mu \left[\frac{\partial^2 u}{\partial x^2} + \frac{\partial^2 u}{\partial y^2}\right] - \frac{\partial P}{\partial x} - \rho g \tag{2}$$

Where P represents the pressure. The x and y correspond with the vertical direction and normal direction through the film, respectively.

In region 1, located far above the bath surface, flow effects are insignificant and film thickness becomes constant with respect to substrate height. In this region, gravity and viscosity forces are taken into account, the surface tension of the liquid is not present, so the equation of motion is simplified as follow:

$$\mu\frac{d^2 u}{dy^2} - \rho g = 0 \tag{3}$$

The no-slip boundary condition at the moving substrate is written as:

$$u = U \quad \text{at} \quad y = 0$$

where U is the substrate velocity and also tangential stress at the interface is insignificant. Integration of equation (3) and applying the boundary conditions leads to obtaining the velocity profile, then the flow rate Q is calculated by an additional integration.

$$Q = \int u \, dy = U \, h_0 \, (1 - \frac{\rho g \, h_0^2}{3\mu \, U}) \tag{4}$$

Where h_0 is the constant film thickness. It is quite evident that the thickness should be a function of the velocity of withdrawal, gravity, and viscosity as well as surface tension which is well-defined as the capillary number.

Many solutions were suggested for finding the constant film thickness in region 1. A well-known model was developed by Landau, Levich, and Derjaguin (LLD theory). LLD law is applicable to a fluid with low Ca. They assumed gravity was insignificant

compared to surface tension, therefore, the film thickness in dimensionless form is defined by introducing the dimensionless number H $= h_0\, (\frac{\rho g}{\mu U})^{1/2}$ (Landau. and Levich, 1942; Derjaguin, 1993)

$$H = 0.944\,(Ca)^{1/6} \tag{5}$$

The more general solution was proposed by White and Tallmadge, taking gravity force into account (White and Tallmadge, 1965).

In region 2, dynamic meniscus region, the film thickness varies with vertical distance, due to viscous and gravity forces, leading to a dynamic meniscus. In this region surface tension, gravity and viscosity forces are involved and the Navier-Stokes is expressed as follows:

$$\mu\frac{d^2u}{dy^2} = \frac{dp}{dx} + \rho g \tag{6}$$

The solution of equation (6) is obtained by integration and applying the no drag and no slip at the interface conditions. The pressure profile is substituted by the Laplace-Young equation and converted into the non-dimensional form using following dimensionless parameters; the thickness of meniscus L $= h\,/\,h_0$ and the height of meniscus $\lambda = x\,/\,h_0$

$$p_0 - p = \sigma c, \quad C = \frac{\frac{d^2L}{d\lambda^2}}{[1+(\frac{dL}{d\lambda})^2]^{\frac{3}{2}}} \ \text{(C in dimensionless form)} \tag{7}$$

$$-\frac{L^3}{Ca}\frac{d}{d\lambda}\left\{\frac{\frac{d^2L}{d\lambda^2}}{[1+(\frac{dL}{d\lambda})^2]^{\frac{3}{2}}}\right\} = 3\,(L-1) - H^2(L^3-1) \tag{8}$$

Equation (8) is a differential equation which used to predict the meniscus profile.

Region 3, static meniscus, located near the bath surface, is dominated by gravity forces and surface tension leading to the formation of the static meniscus. The processes are not affected by the flow and can be described by Laplace's equation of capillary statics (Lee and Tallmadge, 1975)

$$\left\{ \frac{\frac{d^2L}{d\lambda^2}}{[1 + (\frac{dL}{d\lambda})^2]^{\frac{3}{2}}} \right\} = H^2 \, Ca \, \lambda \tag{9}$$

Equation (9) is valid when the thickness of the layer is large, and height is small. The solution of the static and dynamic profile can be matched at the boundary between the two regions. And the location of stagnation point can be calculated by (Lee and Tallmadge, 1973)

$$\frac{h_s}{h_0} = 3 - [\frac{\rho g \, h_0^2}{\mu \, U}] = 3 - H^2 \tag{10}$$

The pioneering work of Lee and Tallmadge predicted the shape and size of meniscus using a one-dimensional model, at the low capillary number. Based on their finding, surface tension, withdrawal velocity, and density affect the meniscus shape and size (Lee and Tallmadge, 1975).

Peralta et al (2014) developed a mathematical model by considering generalized Newtonian fluid (GNF) behavior for dip coating process based on mass and momentum transfer. In the GNF model, viscosity is depending on a shear rate and normal stress and time-dependent elastics effects are not considered. The dip coating problem is solved without considering the surface tension force in the system and applied it mainly to viscosity and gravity forces (Peralta et al., 2014).

At small *Ca*, surface tension is more important than the viscous force and it controls the meniscus shape. On the other hand, at large *Ca* the inertial force come into effect, hence a balance between gravitational, viscous and inertia should be considered to govern the velocity profile. Gravity also plays a key role in the dip coating. Analogously, the Bond number is of order one or more ((Marques et al., 1978; Schunk et al., 1997).

Dip coating is performed in both batch and continuous processes. The continuous coating process is used for long, flexible sheet or filament substrates and the batch process most

frequently used. The frame of reference in which the flat part of the meniscus remains stationary is different between them (Scriven, 1988; Schunk et al., 1997)

1.2 «Effect of velocity»

If the dip coating process is operated at slow speed, the thin film is deposited on the substrate. The solid-liquid interface controls the liquid entrainment. Due to the liquid viscosity, the liquid adjacent to the substrate must move at the same speed as the substrate, adhere to it and then form the film. Simultaneously, the liquid-air interface is deformed as a result of solid withdrawal which is subject to resistance by the surface tension. Therefore, capillary and viscosity forces are considered as the important forces which were defined before as the capillary number Ca.

In order to deposit a thin liquid film on the substrate, the low-speed withdrawal of the substrate from the liquid should be employed. The high-speed withdrawal which is in high demand in the coating industry, leads to deposition of thicker films. Nevertheless, it is considered as one of the drawbacks of dip coating process (Groenveld, 1971).

At high Ca, measurements diverge significantly form LLD theory. Inertia becomes dominant over capillary forces. Inertia cause diverging behavior and thus a delicate balance between inertial, gravitational and viscous forces should be implemented in order to develop the velocity profile (Marques et al., 1978).

If the Weber number (We= $U^2. \rho .r / \sigma$) become more than unity i.e. in high speed, the viscous boundary layer becomes thin and restricts the entrainment. Surface tension does not have any effect on the film thickness. From a practical point of view, in most coating industry the viscous boundary layer regime affects the processes (Quéré, 1999).

1.3   «Effect of fluid rheology»

Dip coating fluids in most cases are non-Newtonian in character. Most coating liquids are suspensions or emulsions which are complex fluids and need further investigation. Newton 's law of viscosity describes the relationship between the velocity gradients and stress component, but it is not sufficient for polymeric fluids and non-linearity is described using generalized constitutive equations. Significant studies have been done in the area of Newtonian fluids. Shear effects and elasticity are the most outstanding characteristics of polymeric fluids. Moreover, the final coating thickness is decreased by elasticity (Tanguy et al., 1984).

1.4   «Bath Geometry»

Kheshgi et al. (1992) had investigated the bath configuration effect in dip coating. They observed that there is a reduction in film thickness, which is the result of moving the bath wall towards the curved part of the meniscus (Schunk et al., 1997). It means the final film thickness is controlled by bath configuration. The flow in the transition zone, between the pool and the developed flow upstream, is influenced by changes in bath geometry and affect the static meniscus as well (Kheshgi et al., 1992).

Javidi and Hrymak (2015) found that the final film thickness decreases with reducing the ratio *R/r* of the bath radius (*R*), and the cylinder substrate radius (*r*) for both Newtonian and non-Newtonian fluids while the process conditions remains unchanged, before reaching a plateau. Withdrawal velocity, physical properties of the coating fluid, substrate geometry and wall proximity have an impact on the final thickness. The substrate is completely wet by the fluid and it moves with a constant value of the withdrawal speed. Their finding verified that wall effects can alter deposited film thickness and the position of the stagnation point during dip coating processes. (Javidi and Hrymak, 2015).

Most of the pioneering research of dip coating assumed that the pool of liquid is large enough so as not to consider the reservoir wall effect on coating film thickness. The film thickness in the confined dip coating is different at specific bath sizes from film thickness

in unconfined dip coating at the same conditions such as withdrawal speed and liquid properties. In the confined liquid pool, the meniscus has more curvature than in an unconfined case because of the presences of the stationary wall. Capillarity affects the curvature increase and therefore adjusts the force balance in the dynamic meniscus region. A channel is created between the moving substrate and the stationary wall. Depending on the capillary number, two separate flow regimes are generated: the meniscus-controlled regime for low Ca and the channel-controlled regime for high Ca (Kim and Nam, 2017).

Figure 3 shows these two regimes; in the meniscus-control regime, except in region 1 and 2, the liquid is almost quiescent and for the channel-controlled regime, the dynamic meniscus region 2 occupied the channel and the stationary pool vanishes. (Kim and Nam, 2017).
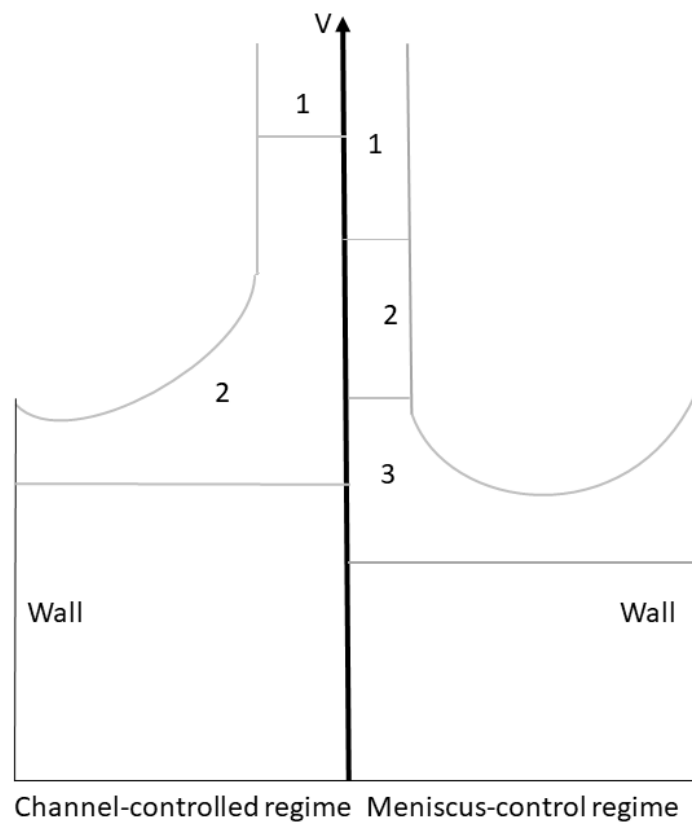
Figure 3: Schematic of the confined dip coating process in high and low Ca

The channel-controlled regime or high Ca, the viscous force transferred from a moving substrate is considerably large so make the contact line in the motion on the stationary wall, in another word, the contact line moves along the wall.

The meniscus-controlled regime or at the low capillary number, the film entrainment and static regions are connected by dynamic meniscus regions. In fact, the force balance in the dynamic meniscus region specifies the flow rate through the film entrainment. The radius of meniscus curvature is comparable to half of the channel width in the static meniscus region (Blake and Ruschak, 1979; Krechetnikov and Homsy, 2006).

1.5 «Numerical Modeling»

Similar to many technologies and sciences, performing computational mathematics with high-speed modern computer became the inseparable component of the coating process and its research and development.

Analyzing coating processes need advanced numerical methods for solving the continuity and transport equations and its boundary conditions for free surface flows. Usually, the existence of the free surface condition in a system makes it more complicated (Stephan F. Kistler, 1997)

Many of the advances in numerical solutions have relied on finite-element techniques. The governing equations are discretized on boundary-confining meshes which adjust independently to changes in the flow geometry. Finite element discretization and boundary associated meshes make the calculations with free surface conditions much easier. (Amsden, 1980).

During the dip coating process and film formation, momentum, heat and mass transfer occur but in many practical applications, the isothermal and non-evaporative conditions are relevant. Accordingly, the problem will be simplified to the study of the fluid dynamic problem alone.

Tanguy et al (1984) simulated the dip coating processes using the finite element approach and applied the Galerkin method coupled to discontinuous pressure element discretization of the continuum. In this method, the complex axisymmetric flow situation includes the free surface and the stagnation point are predicted.

While LLD theory provides a good prediction for steady state flow with a small capillary number, it cannot be used for other regimes, i.e. unsteady flows. Jenny and Souhar, (2009) developed a two-dimensional simulation applying Arbitrary Lagrangian Eulerian (ALE) formulation and full steady-state Navier-Stokes equations and a tracking method for the moving free surface (Jenny and Souhar, 2009).

In this study, GOMA 6.0 a full-Newton finite element program is employed. GOMA solution is based on the full Newton-Raphson iterative scheme for the discretized finite element equations, which can provide for simultaneous solution of all active equations and boundary conditions in a single matrix. Furthermore, it is ideally preferred in order to solve problem containing coupled bulk mechanics and interfacial phenomena. Moreover, GOMA provides outstanding tracking of the free and moving boundary formulations. the fully implicit, pseudo-solid, unstructured mesh deformation algorithm and ALE algorithms distinguish GOMA from any other finite element programs (Schunk et al., 2013).

1.6 « Scope of the Research »

The main objective of this research is to study the distribution of noncolloidal particles in suspension in the coating film region in the dip coating process. Several parameters take into consideration in order to elaborate their effect. These parameters include the wall proximity, particle concentration, particle radius, and withdrawal speed. The addition of particles to a Newtonian liquid modifies the rheological behavior of the fluid. The shape and the position of the interface, as well as the final film thickness are also affected as a result.

Complex phenomena in suspension flow happen as a result of particle-particle interactions, which cause the shear-induced migration and particle arrangement based on flow kinematics. Strong migration of particles occurs as a consequence of high shear rate gradient; accordingly, the particle concentration varies in the flow field. In addition, it is of significant interest to predict the particle concentration changes in the coating film. The model in this study is implemented for the two-dimensional case. The Galerkin finite element method (FEM) is employed for the discretization of the transport equations for the free boundary problem.

To the best of the author's knowledge, there are few studies in the literature devoted to studying the particle distribution in the coating film particularly in the dip coating process. Fundamental literature related to the dip coating process dates back for decades. Studies of the particle migration during the dip coating processes is of significant interest in recent years and addressed in the second chapter. The case of solvent evaporation and drying (vitrification) is not addressed in this work, nor are the effects of surface tension modifying agents (e.g. surfactants) included in the studies .There is literature for particle suspensions in slot coating flow (Rebouças et al., 2018), but the free boundary characteristics of slot coating and dip (withdrawal) coating are quite different.

1.7 «Thesis Outline»

Chapter 1 commences with a concise introduction of the dip coating process and summarizing the most impactful factors involving in the process include fluid rheology, withdrawal velocity as well as bath configuration effect.

In chapter 2, the references affiliated with the concentrated suspension used in dip coating processes are presented. The convective self- assembly as a desirable technique for creating deposition of a patterned particle on the substrate is discussed and the hydrodynamic of dip coatings in the fluid-particle system is articulated.

In chapter 3, the numerical calculations of the dispersed solid particles in the coating fluids are developed by implementing a GOMA 6.0 solver. Simulation of particle

distribution in free-surface suspension using the finite element method is employed and the effects of the coating bath walls near to the substrate are investigated. A continuum constitutive equation based on the diffusive flux model is used in two-dimensional flows. The solid capability of the solver to capture the free surface provide the effect of the wall on the interface morphology.

Finally, the conclusions and recommendations for future work are given in chapter 4.

Chapter 2

2 « Literature Review»»

Most of the research in the area of coating processes consider coating flow as a simple Newtonian liquid while in coating industry application, most liquids are particle suspensions, polymer solutions and polymer melts that show significant non-Newtonian characteristics. The microstructure of deposited film generated from concentrated suspension is discussed in this section

2.1 «Introduction»

2.1.1 «Shear-induced migration in concentrated suspension»

A thorough flow model associated with the suspension of particles is required for the purpose of determining the flow characteristics and microstructure of liquid flow in the deposited film. Since the majority of liquids used in coating processes show non-Newtonian features, which consist of a viscous liquid medium with rigid particles suspended throughout the fluid. The rheology of the suspension heavily relies on the microstructural organization of the particulate solid phase and solvent properties (Krieger, 1963; Krieger, 1972).

Suspensions often show non-Newtonian rheological behavior, which includes shear-thinning or shear-thickening. Shear thinning (i.e. viscosity reduction) happens as a result of damaging the accumulation and microstructures alignments, by way of contrast, shear thickening (i.e. viscosity increase) occurs due to the solid contacts among particles in clusters that are subject to jamming or chaotic transition. (Hoffman, 1972)

A well-known phenomenon in concentrated suspension is shear-induced particle migration where particles migrate to and along the streamlines under the inhomogeneous shear flow. The particle transportation occurred due to shear rate gradients and variations in suspension viscosity due to irreversible particle-particle interactions (Gadala-Maria,

1980; Leighton and Acrivos, 1987a). The complexity of coating flow results in the movement of particles in the shear-induced flow and causes disorder in the distribution of particles.

Several experiments have reported particles migration in initially homogenous suspension to the low shear rate regions in shear flows. Maria and Acrivos (1980) measured viscosity in the Couette viscometer and observed viscosity of the concentrated suspension of neutrally buoyant particles in a Newtonian fluid under the action of shear shows a reduction whilst there is no change in pure suspending viscosity with the same condition (Gadala-Maria and Acrivos, 1980).

Leighton and Acrivos (1986) demonstrated that this phenomenon happens because particles under the action of shear migrate out of the sheared Couette gap and move into the stationary fluid reservoir. The schematic of Couette viscometer is shown in Figure 4. As a result, the particle concentration in the gap decreases and therefore decrease in observed viscosity. Following experiments also discovered an instant rise in the viscosity when a suspension in a Couette device initially is sheared. This is attributed to the particle migration across the gap width. A short-time increase and then long-time decrease in viscosity lead to obtaining the value of shear-induced diffusion coefficients. These coefficients are of significance to govern the particle concentration profile in shear flow. In this flow, convective diffusion dominates the particle migration in direction of the fluid. Consequently, diffusion along the velocity gradients which is normal to the direction of fluid motion, lead to governing their magnitude.

torsion shaft

couette gap

bob

reservoir

cup
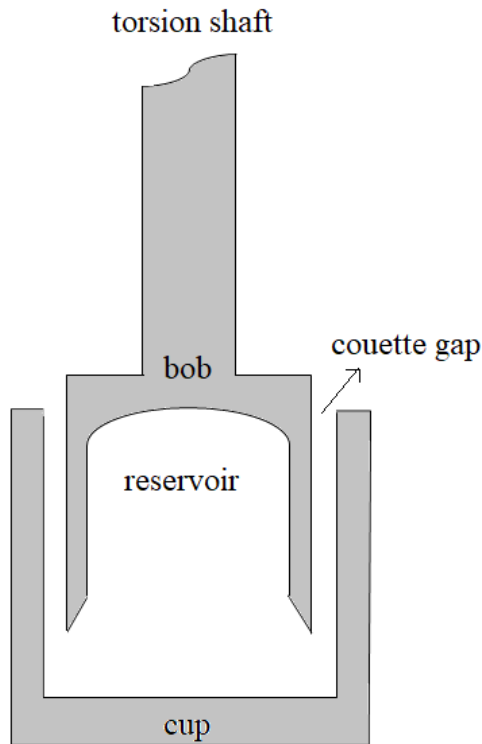
Figure 4: Schematic diagram of a Couette device

In addition to the experimental part, the theoretical investigation proved that irreversible interparticle interactions take place in these suspensions resulting from the particle migrations (Leighton and Acrivos, 1987b).

They also developed an experimental method to measure the shear-induced coefficient of self-diffusion which is a function of concentration, shear rate, and particle radius. Self-diffusion is defined as the random movement of particles in flow and happens because of the simultaneous interactions between particles. The coefficient is proportional to the square of the particle radius, square of concentration in the dilute system and shear rate as well (Leighton and Acrivos, 1987a; Phillips et al., 1992).

The properties of the suspension fluid, where there are shear-induced viscosity changes completely differing from the Newtonian case, and so study of the particle distribution (particularly in free surface problems) is of significance to process improvement.

In a solid-liquid suspension, particles migrate under shear stress gradients. To be more exact, in initially well-mixed suspension, small particles migrate, from regions of high strain rate to regions of low strain rate (Leighton and Acrivos, 1986). Modeling of this migration at the microscopic scale is restricted due to the tremendous amount of computing resources for calculation of individual particle motion in a suspension in an industrial process (Abbott et al., 1991; Brinker et al., 1992).

A thorough examination of shear-induced phenomena was done by Phillips et al (1992), with a developed constitutive equation for particle flux in one dimension. Two-dimensional flow investigations in circular Couette flow were performed by Phan-Thien and Fang (1996). Their numerical modeling of particle migration in concentrated suspensions used the finite volume method. The numerical predictions showed that particles in an eccentric circular geometry migrated at dissimilar velocities towards the outer cylinder (region of low shear rate) (Phillips et al., 1992).

Lyon and Leal (1998) performed an experimental study in a two-dimensional channel flow for mono-disperse particle systems and demonstrated that the particle concentration distribution has a maximum near the channel centerline and a minimum at the channel walls. Particle velocity varies across the channels in which had the sharp maximum at the location of approximately 20% from the channel axis in direction of the walls (Lyon and Leal, 1998).

In suspension problems, assuming a uniform distribution of particle in many industrial applications is not applicable (Ritz et al., 2000). Creating a uniform, defect-free coating structure on a substrate is useful in product development. Vertically withdrawing a substrate from a solid-liquid suspension is one of the inexpensive approaches that can produce patterned microstructures. The solid-fluid suspension is being utilized in industries such as composite materials, pharmaceutical, environmental, paper coatings, paints, cosmetics and biological fields (Tadros, 2011).

 Most of the studies dedicated to extending equations in these complex multiphase systems relate the bulk rheology to the volume fraction of particles and Brownian and colloidal forces with the assumption of particle distribution being uniform throughout the

domain (Mukhopadhyay et al., 2009). Although the hydrodynamics of the process depends on the uniform distribution of particles, the assumption is unfounded in many applications (Mewis and Wagner, 2012).

2.1.2   «Free-surface flows of particle suspensions»

It is worth mentioning that the studies cited previously have been restricted to channel or closed conduit flows while in many industrial applications, such as continuous coatings, deal with suspension in free surface flows where there are a few studies. As stated before, the presence of the free surface flow in the process adds more complexity to the suspension problems.

The first research in this area was done by Husband et al (1994) which investigated the suspension flow of bimodal particles in different geometries. They observed that small particles migrate slower than coarse particles, which lead to segregation and also they move to the free surface where the shear rate is low (Husband et al., 1994).

When the particle size is greater than one micrometer, inter-particle potentials and Brownian forces are not considered influential forces for determining the macroscopic behavior of suspensions rheology of solid particles in Newtonian suspending fluids. The linearity of the final equation for fluid motion with negligible inertial effects circumstances lead to projecting the linearity of total stresses in a suspension of smooth non-Brownian spheres. The result of this situation is that either shear thinning, or shear thickening are identified. (Min and Kim, 2010).

Min and Kim (2010) probed free surface flows of suspensions in slot coating and a planar jet flow using the diffusive flux model by finite element technique in order to track particle migration. Their results demonstrated that the velocity profile was fully developed; however, the particles were not distributed uniformly. Inertia effect, suspension concentration, and particles size were also discussed. The small size of particles causes them to be more depleted of areas adjacent to the free surface (Min and Kim, 2010).

A few studies investigated particle suspensions in free-surface coating, particularly in dip coating processes. Campana et al (2017) implemented the finite element approach and solved the equations of momentum linked to the equation defining the particle transport to examine non-colloidal suspension flow of rigid spherical particles in slot coating. Their main finding indicates that the distribution of the particle in the final layer is extremely disordered, which stems from shear-induced migration and operating parameters (Campana et al., 2017).

Campana et al. (2017) analyzed the particles distribution of concentrated suspension in slot coating flows and found that operating parameters such as imposed flow rate affects the particles distribution in coated film and it is non-uniform (Campana et al., 2017).

2.2 Influence of particle suspension and flow characteristics»

At steady state conditions, the suspension particle concentration, Reynolds number, and particle Peclet number are the main factors used to specify the viscosity of the particle suspension assuming the particles are neutrally buoyant. To shed more light on this matter, the Peclet number defines the competition between Brownian forces and viscous forces (Stickel, 2005).

For non-colloidal suspensions, where Reynolds number is insignificant (Re → 0) and the Peclet number is very large (Pe → ∞), (Pe = $a^2\dot{\gamma}$/ D), where D is the particle Stokes-Einstein diffusion coefficient, $\dot{\gamma}$ is the local shear rate, and the radius of the particle is represented by a. Under these conditions, the non-viscous forces and inertia are considered insignificant, accordingly, the viscosity of suspension can be defined as a function of the volume fraction. (Stickel, 2005; Hinch, 2011).

2.3 «Review of the convective assembly of patterned particle deposits»

Ordered arrays in multi-dimensional structures consisting of particles assemblies on substrates have been observed in a multitude of applications. These applications include: novel optics (Joannopoulos et al., 1997), chemical (Holtz and Asher, 1997; Asher et al., 2003), microelectronics (Hayashi et al., 1991), biochip devices (Fiegel et al., 2005), sensing (Holgado et al., 1999) and data recording platforms (Holtz and Asher, 1997), data storage, templates for nonlithographic patterning (Velev et al., 1997) and the creation of ordered microporous materials (Zheng et al., 2002), surface coatings, selective solar absorbers (Hahn and Seraphin, 1978), in addition to templates for the creation of nanostructured (Sun et al., 2007) or ordered porous materials (Park and Xia, 1998). From an industrial viewpoint, the self-organization of particles is considered as the most important aspect of product performance (Watanabe et al., 2009) (Dimitrov and Nagayama, 1996).

Numerous approaches have been applied to prepare ordered assemblies in order to meet the challenge of future technology. To name a few of these techniques, it is noteworthy to refer to the Langmuir-Blodgett method, placing of particles by electrostatically deposition, and gravitational sedimentation.

By performing a dip coating procedure, ordered aggregates of particles are deposited on the solid surface. By considering the smooth and energetically homogeneous solid surface, particles are deposited on the substrate in a way that the predominant flow field convects them to the three-phase contact line. Well- organized crystalline structures form by inducing the particles when capillary bridges are shrunk. (Denkov et al., 1992; Dimitrov and Nagayama, 1996)

A spontaneous alignment of particles on a solid plate can be achieved from a suspension of particles and the substrate vertically withdrawn from the fluid. While the plate is kept immobile, various layers of particles initiate to be shaped spontaneously over the surface, covering an area between the contact line all the way to the bulk suspension. Particles arrays are formed without interruption or gaps to a different size when the withdrawal

velocity and array formation rate equal. Indeed, the particle structures formed based on film geometry. There will be an expansion in the thickness of the film starting from the contact line and extending to the bulk suspension. Therefore, monolayers, bilayers, multilayers are likely to form with the flux of particle covering the area between the surface of the film and the substrate (Dimitrov and Nagayama, 1996).

Despite the other methods, the colloidal crystal nucleation takes place merely around the meniscus apex including convective relocating of particles coming from the suspension bulk to the coating film and the meniscus (Colosqui et al., 2013). Controlling the motion of meniscus can lead to the additional formation of well-ordered structures (Watanabe et al., 2009).). Implementing the spin-coating technique is another method for arranging thin particle layers, this technique involves a suspension of small particles covering all across a rotating substrate (Dimitrov and Nagayama, 1996).

In an experiment with polystyrene spheres and mercury, it was observed that lateral capillary forces can gather the particles into layered arrays so electrostatical lateral capillary forces are in control of interactions between particles in films. In the condition of saturated atmosphere with water vapors, the particles assemble extremely slowly into array nuclei. Suspension influx drives the particles into the thinner film's areas and lateral capillary immersion forces cause them to attract each other, accordingly, small hexagonal aggregates parts will be formed. The aggregation of particles in a different orientation is constrained in the leading edge of arrays. Constraining the capillary menisci towards the substrate hindered additional particles alignment. In the wetting film, with a thickness approximately the size of particle diameter, the particles coming near to the leading edge of the array do not attach one another because of the forces of immersion. Hydrodynamic flux constrains them separately, so they discover unoccupied positions in the growing areas (Dimitrov and Nagayama, 1996).

If there is an increase in the line tension linked to a contact line with three-phase, near the spherical solid particle, the contact angle located between the interface and particle will not expand from zero to 180. Instead, a disjoined drying- wetting transition might be created on condition that the critical value is obtained, In fact, this transition happens

where the energy of the particle immersed into a bulk phase is equal with the particle located at local equilibrium on the interface. It is also worth noting that the local equilibrium in an interface is very likely to occur for line tensions with a higher value than that needed for the transition. In other words, for irreversible removal of the particles from bulk phases an activation energy is necessary (Aveyard and Clint, 1996).

Substrate withdrawal speed and evaporation rates are considered as two controlling factor that creates uniform crystalline structures over areas of large extent (Dushkin et al., 1999; Jiang et al., 1999).

The capability of producing a pattern structure on more complicated surfaces like soft, confined or curved substrate contributes to creating novel and smart materials. The colloidal crystallization characterized by Abkarian et al (2004), was located in circular capillaries. A confined capillary meniscus applied on colloidal packing by a wedge-like region can produce striped ring patterns consisting of particle. That patterns are spontaneously shaped in a cylinder. Their finding demonstrated that the width and the spacing between periodic colloidal deposition increase with particle concentration and they decline in time in the capillary (Abkarian et al., 2004).

Marangoni-Benard instability in both aqueous media and organic solvents has led the pattern deposition of particles (Nguyen and Stebe, 2002). Also forming of periodic structures has been developed by periodic contact line pinning and jumping (Adachi et al., 1995; Ray et al., 2005).

One means of creating the well-ordered assemblies, which received extensive attention, is convective self-assembly. This method is widely employed because of its simplicity and compatibility. In this technique, ordered colloidal crystalline assemblies formed by using interactions between particles throughout the suspension encompassing the balance of van der Waals and electrostatic interactions as well as depletion interactions and gravitational effects. The applied configuration for this method is dip coating in which there is vertical immersion in the suspension fluid. This method can produce patterned microstructures that cover the substrate over millimeter lengths. Subsequently, on the

substrate surface a colloidal crystalline film is formed when it is withdrawn from the particle suspensions (Fan and Stebe, 2005; Huang et al., 2005; Ghosh et al., 2007)).

As long as the solid substrate has a patterned structure, the contact line sweeps the particles into cavities as the suspension gradually falls back. Particles can deposit in an orderly manner even on energetically homogeneous substrates. Marangoni-Bernard convection can drive particles into a connected network of polygons structures (Yin et al., 2001; Nguyen and Stebe, 2002; Cui et al., 2004; Juillerat et al., 2005; Li et al., 2005).

Ghosh and Stebe (2007) examined the formation of periodic stripes on a uniform surface using dip coating configuration. Withdrawal speed U corresponding to a transition speed U_t (150 µm/min) changes the stripe width and spacing. While the velocity is less than the transition velocity (10 µm/min), gravity dominates and widen the stripes with large spaces between them. However, for high-speed velocity ($U > U_t$) 160 µm/min the width becomes narrower by small spaces between them. At transition velocity, a thin liquid film entrained atop of the meniscus. Because of the large size of the particles, they agglomerate in the region between the meniscus and the film. In very high speed i.e. 2 cm/min, since the entrained film is sufficiently thick, particles convected directly into the film with no ordered deposition (Ghosh et al., 2007)

The final structures have various scales in length including the particle length, scale of colloidal aggregate as well as particles-rich and particle-poor areas. Several methods have been employed in order to generate periodic structures. To create spontaneously pattern colloidal structures, physicochemical or mechanical instabilities in suspension are utilized. (Borchers et al., 2005; Burkert et al., 2007).

2.4 Hydrodynamic of dip coatings in the fluid-particle system»

It has been demonstrated when the speed of withdrawal is less than a critical speed, periodicity and regularity of the particle structure is significantly improved. At the critical speed, the thickness of coating film is equal to particle diameter (Landau. and Levich, 1942) and set the upper limit of the thin-film entrainment regime (Ghosh et al., 2007). Hydrodynamic interactions between colloidal particles significantly affect the self-organization processes. Brownian effects and long-rang molecular interactions between solid parts are ignored (Watanabe et al., 2009).

During the withdrawal of a plate, the generated two-dimensional flow drives the particles from bulk to the meniscus part and then to the coating film shown in Figure 5. A homogeneous distribution of particles along the direction of the strip requires for developing the periodicity and regularity of the strips. Considering two-dimensional flow configuration similar to Landau-Levich simplified the process (Colosqui et al., 2013).
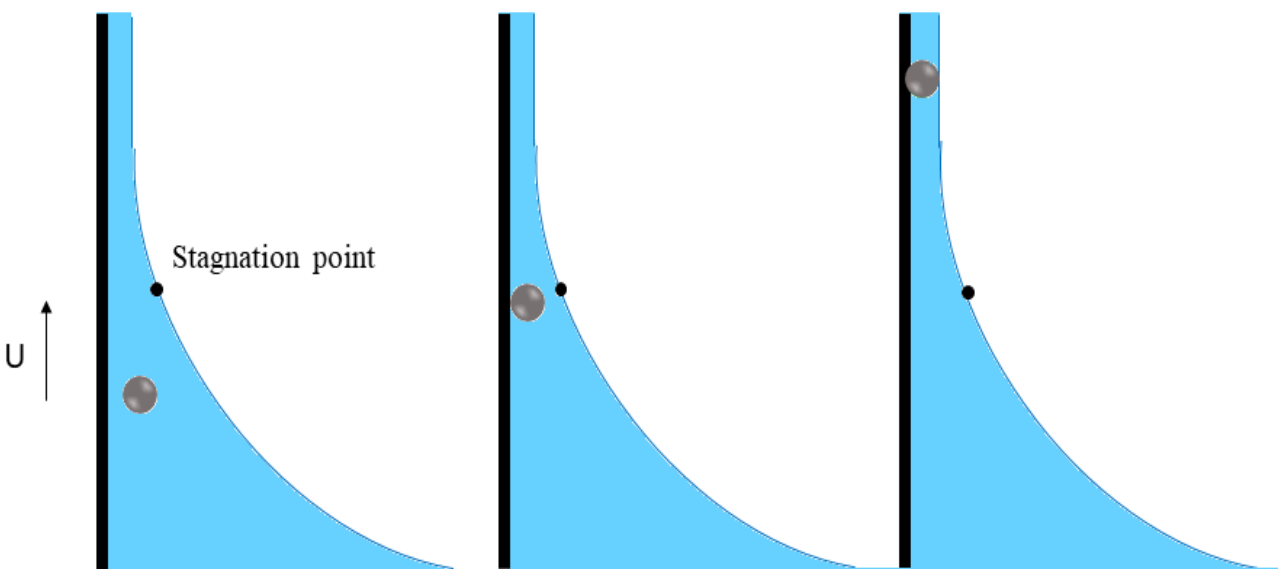

Figure 5: Single particle displacement during the dip coating process

Watanabe et al (2009) probed into stripe pattern formation by utilizing the convective assembly technique along with examining some experimental parameters effects including particle concentration, withdrawal speed, solvents and material of the substrate. They found that in the quasi-static process, a very low concentration of particles leads to well-defined stripes, which spontaneously form at the three-phase contact line. Withdrawal speed, particle concentration and surface tension influence the width of stripes. Whereas surface tension impact on stripe spacing. The stripe spacing decreases with the decrease in the surface tension. Stripe become wider with increasing the concentration and withdrawal speed and have a little dependency on the surface tension. Also, the stripe width and the following spacing have a direct relation, such that wider stripe located subsequent to wider spacing. Stripe formation and stripe spacing are defined by the curved shape of the meniscus.

Where the concentration of particles is high, the flux of particles is sufficiently large and lead to the formation of the continuous film. On the other hand, in low concentration condition, the flux would be lower so the rate of particualte film formation cannot comply with the substrate velocity. The difference in rate create the distances. Meniscus shape becomes concave to satisfy the Laplace equation in static meniscus as shown in Figure 6. The particle flux decrease since the liquid path thins so slows the elongation and curves the meniscus. Then the width narrows such that particles cannot pass. That leads to the stripe formation. (Watanabe et al., 2009).
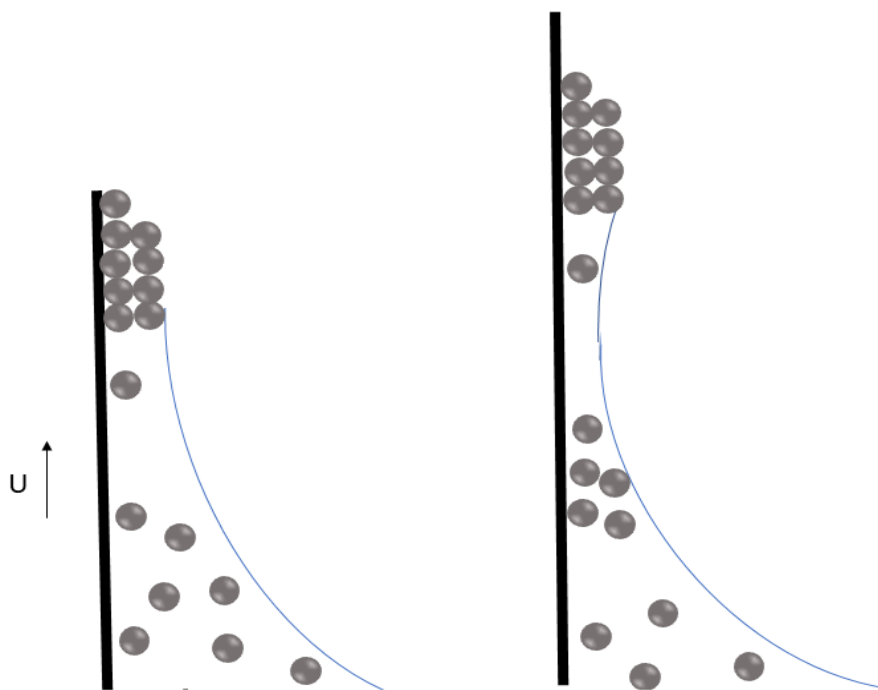
Figure 6: Stripe pattern formation on the fully wet substrate

Simulation of a number of particles (N=10-20) confirm the theory of the periodic formation and ordered deposition. Particles are released from random locations. The results showed that the particles assemblies produce before they enter the film. This occurrence caused more periodic and ordered arrays form. By increasing the withdrawal velocity and area fraction, disordered assemblies form in the coating film. This happens since long-ranged capillary interactions and film instabilities drive assemblies which deteriorates the periodic and ordered arrays (Kralchevsky and Nagayama, 2001; Colosqui et al., 2013).

Chapter 3

3 « Modeling of the Dip Coating for Dispersions with Near Wall Effects »

3.1 Abstract»

Numerical study of a suspension in the dip coating process is studied in this chapter. An infinite length substrate is pulled out from a suspension of neutrally buoyant hard spheres particles. The suspension is considered as a Newtonian fluid with a concentration-dependent viscosity. Numerical simulation of particle distribution in free-surface suspension using the finite element method is employed and the effects of the coating bath walls near to the substrate are investigated. A continuum constitutive equation based on the diffusive flux model is used in two-dimensional flows. The understanding of particle distribution in the liquid bath, particularly near the free surface and substrate, under different conditions inform the improvement of the process operation and quality

3.2 «Modeling Approach »

In this study, Goma 6.0 a full-Newton finite element program was used. The Goma solution procedure is based on the full Newton-Raphson iterative scheme, which can operate a simultaneous solution for all active equations and boundary conditions in a single matrix. Furthermore, it is ideally preferred in order to solve a problem containing coupled bulk mechanics and interfacial phenomena. Furthermore, Goma allows surface tracking in free and moving boundary formulations. The fully implicit, pseudo-solid, unstructured mesh deformation algorithm and ALE algorithms distinguish Goma from other finite element programs (Schunk et al., 2013).

The particle distribution as a continuum phase in concentrated suspension is examined. A constitutive equation in Goma 6.0 finite element program is implemented in order to study the behavior of the fluid during the dip coating process. The diffusive flux model based on Phillips et al (1992) for a concentrated suspension system has been applied. The

simulation case is the flow behavior of suspensions composed of large, monodisperse, spherical particles using a Galerkin/finite element discretization, and the Navier-Stokes equations.

3.3 «Numerical Modeling»

3.3.1 «Development of Constitutive Equation»

A modeling approach for a suspension containing neutrally buoyant particles in quiescent and flotation setting has been developed (Phillips et al., 1992; Zhang and Acrivos, 1994). This model was developed to predict the evolution of particle concentration profiles over time. In the following sections, the equation used for the suspension density and viscosity is presented as well.

The assumption of $a \ll L$ in the constitutive model is considered. Where L is the characteristic length and a is the particle radius (Phillips et al., 1992). In the dip coating process, the characteristic length is the dimensionless film thickness

$$l_c \equiv \sqrt{\frac{\sigma}{\rho g}} \quad \text{or} \quad l_f \equiv \sqrt{\frac{\mu u}{\rho g}} \quad \text{(Kim and Nam, 2017)}.$$

These numbers are calculated as follow $l_c = 1.75 \times 10^{-2}$ and $l_f = 3.8 \times 10^{-3}$. Having the particle radius of 6×10^{-5} m, the assumption of diffusive flux model is met.

3.3.1.1 «Density»

The density of the suspension depends on the local particle concentration because carrier fluid and solid particles have different densities. Where ρ_f and ρ_s are the mass concentration of the fluid phase and particle phase, respectively, therefore:

$$\rho_f = (1-\varphi) \, \rho_f^0 \tag{1}$$

$$\rho_s = \varphi \, \rho_s^0 \tag{2}$$

φ is the volume fraction of solid particulate phase and ρ_f^0 and ρ_s^0 are the pure phase densities so the total mixture density is defined by following relationship:

$$\rho = \rho_f + \rho_s = \rho_f^0 + (\rho_s^0 - \rho_f^0)\, \varphi \tag{3}$$

Therefore, particle concentration has an impact on suspension density which can vary through the entire suspension. Consequently, the variation of total density results in to introduce buoyancy-driven flow source term in the momentum equation (Rao et al., 2002).

3.3.1.2 «Viscosity»

One of the first attempts among the various approaches for developing the viscosity of dilute suspension in a Newtonian fluid was by Einstein. He derived an equation based on energy dissipation in a sphere with radius R around the particle as R→ ∞. Certain flow field adjacent to the surface of the particles leads to computing supplementary energy dissipation that stem from the existence of particles. Recognized (corrected) Einstein relation is as follow:

$$\mu = \mu_f(1+2.5\ \varphi) \tag{4}$$

where μ denotes viscosity and φ is the particle volume fraction.

On condition that no non-hydrodynamic inter-particle forces exist, it follows from the dimensional analysis that the relative viscosity of the suspension as a Newtonian fluid depends on the volume fraction of solids; One commonly used relative viscosity is the empirical Krieger-Dougherty equation, in which $\mu = \mu\ (\varphi)$ at Pe>>1 (Krieger, 1972).

$$\mu_r = (1-\varphi/\varphi_m)^{-1.82} \tag{5}$$

Where $\mu_r = \mu\ /\ \mu_f$ is the relative viscosity (μ_f is pure fluid viscosity)

φ is the volume fraction, and φ_m is the maximum packing particle concentration and consider of order 0.68 for hard spheres ($\varphi_m = 0.68$) as μ_r tends to infinity. So, the behavior of viscosity is nonlinear and depends on particle concentration. It changes from highly viscous solid-like at the limit of maximum packing φ_m to lower region in the pure fluid. (Krieger, 1972).

3.3.1.3 «Governing equation»

The momentum equation is developed assuming that the viscosity is dependent on the local particle concentration via the Krieger model. Most of the following notations are adapted from (Rao et al., 2002).

$$\rho \frac{\partial v}{\partial t} + \rho v.\, \nabla v + \nabla p - \nabla . \left(\mu(\nabla \upsilon + \nabla \upsilon^t) \right) - \left(\rho_f^0 - \rho_s^0 \right) \varphi g = 0 \tag{6}$$

where v and P represent the suspension velocity and dynamic pressure respectively, g is the gravitational acceleration, and t is the time. Dynamic pressure has absorbed the constant portion of the momentum source which leads to generating further stability in numerical implementation for buoyancy driven.

The full continuity equation is applied as the total density is not constant and varies with local volume fraction:

$$\frac{\partial \rho}{\partial t} = - \nabla . (\rho \, \upsilon) \tag{7}$$

By substituting Equation (3) for density, the divergence of velocity in terms of an equation for particle volume fraction achieved:

$$\rho_f^0 \, \nabla . \upsilon = \Delta \rho \left(\frac{\partial \varphi}{\partial t} + \nabla . (\upsilon \, \varphi) \right) \tag{8}$$

The expression in parentheses of Equation (8) is named as particle flux

$$\frac{\partial \varphi}{\partial t} + \nabla . (\upsilon \varphi) = \frac{1}{\rho_s^0} \nabla . J_s \tag{9}$$

The source term in the continuity equation based on non-constant density is calculated by substituting Equation (9) into Equation (8):

$$\nabla . \upsilon = \frac{\left(\rho_s^0 - \rho_f^0\right)}{\rho_s^0 \rho_f^0} \nabla . J_s \tag{10}$$

The particle flux in a standard form is given as follows,

$$\frac{\partial \varphi}{\partial t} + \nabla . (\varphi \, v) = - \frac{\nabla . J_s}{\rho_s^0} \tag{11}$$

If we substitute Equation (11) into Equation (10) instead of divergence velocity, thus

$$\frac{\partial \varphi}{\partial t} + \upsilon . \nabla \varphi = - \left(\frac{\rho_f^0 + \varphi \, \Delta \rho}{\rho_s^0 \rho_f^0}\right) \nabla . J_s = - \frac{\rho}{\rho_s^0 \rho_f^0} \nabla . J_s \tag{12}$$

The particle flux J_s is defined by transporting particles from high shear rate region to low shear rate, concentration variation, viscosity, and gravity.

$$\frac{J_s}{\rho_s^0} = -\left(\varphi \, D_\varphi \nabla(\dot\gamma \, \varphi) + \varphi^2 \dot\gamma D_\mu \nabla (\ln \mu)\right) \tag{13}$$

D_φ and D_μ are diffusion coefficients and should be fit to data using the particle radius squared. (Tetlow et al., 1998)

$$D_\varphi = K_c a^2 = 0.41 \, a^2 \tag{14}$$

$$D_\mu = K_\mu a^2 = 0.62 \, a^2 \tag{15}$$

The diffusion coefficients were determined based on a set of experimental measurements in the Couette device. K_c refers to the particle collisions and K_μ refers to the gradients in the relative suspension viscosity. The ratio of constant values ($K_c / K_\mu = 0.66$) was important in their experiment. The flow in the Couette device depends on this ratio while the individual magnitudes of Kc and Kµ were not important.

These two coefficients are calculated on each section depends on the subsequent conditions.

$\dot{\gamma}$ is the shear rate tensor and is directly related to the second invariant of the shear rate tensor and defined in the standard way (Bird et al., 1960):

$$\dot{\gamma} = (\nabla \upsilon + (\nabla \upsilon)^t) \tag{16}$$

The magnitude of shear rate second invariant is calculated by:

$$E = \sqrt{\frac{1}{2}(\dot{\gamma} : \dot{\gamma})} \tag{17}$$

3.3.2 «Discretization by finite element method»

The momentum Equation (6), the continuity Equation (7), the particle conservation Equation (9), and the shear rate invariant Equation (16) are discretized with the Galerkin finite element method. Velocity, pressure, volume fraction and the scalar shear rate invariant are unknowns. (Donea, 1984).

In incompressible flow, the velocity and pressures should meet the Ladyzhenskaya–Babuska–Brezzi (LBB) conditions. In LLB condition the velocity interpolant should be of higher order than the pressure interpolant. For the two-dimensional problem, the pressure is approximated in linear or bilinear continuous.

$$p \approx p_h = \sum_{i=1}^{m} p_i \psi_i(x) \tag{18}$$

$\psi_i(x)$ is the pressure shape function. Biquadratic shape functions interpolate the velocity unknown.

$$v \approx v_h = \sum_{i=1}^{n} v_i \phi_i(x) \tag{19}$$

Where v defined as true velocity solution, v_h is the approximate finite element solution. v_i denotes the velocity at node i and ϕ_i represents the velocity basis function related to node i. For shear rate magnitude and particle volume fraction no condition exist so bilinear shape functions are applied.

$$\varphi \approx \varphi_h = \sum_{i=1}^{m} \varphi_i \zeta_i (x) \tag{20}$$

$$\dot{\gamma} \approx \dot{\gamma}_h = \sum_{i=1}^{m} \dot{\gamma}_i \xi_i (x) \tag{21}$$

The residual equation is formed by substituting the trial function equation 18 to 21 into the differential equations. For example, the momentum residual R^m :

$$R^m = \rho\frac{\partial v_h}{\partial t} + \rho v_h.\nabla v_h + \nabla p_h - \nabla . \left(\mu_r(\nabla v_h + \nabla v_h{}^t)\right) - \left(\rho_f^0 - \rho_s^0\right)\varphi_h\,\text{g} \tag{22}$$

Weight functions are multiplied by the residual equations and integrated over the domain to find non-linear algebraic equations for the nodal coefficients. In the Galerkin finite element method, the weight functions are selected to be the shape functions. The nodal unknowns are found in this step. The vector momentum equation is weighted for each component of the velocity vector which results in the calculation of volume integral over V. The e_β defines as the unit vector in the coordinate directions (Cairncross et al., 2000).

$$\int_V \phi_i e_\beta. \rho \frac{\partial v_h}{\partial t} + \rho v_h.\nabla v_h + \nabla p_h - \nabla .\left(\mu_r(\nabla v_h + \nabla v_h{}^t)\right) - \left(\rho_f^0 - \rho_s^0\right)\varphi_h\,\text{g}\, dV = 0 \tag{23}$$

The nonlinear problem is solved with Newton–Raphson linearization scheme with an initial guess or previous solution. All equations are solved simultaneously in one Jacobian matrix and then Gaussian elimination solved the large matrix equation to obtain a new solution. This has been shown as an effective and efficient approach for solving large three and two-dimensional problems (Cairncross et al., 2000).

3.4   «Simulations of a concentrated suspension»

Simulation of dip coating of an infinite substrate is presented in this section. Mineral oil is selected as a suspending fluid and spherical polystyrene particles. The size of the polystyrene particle is chosen large enough as it to not exhibit Brownian motions and also small enough to have a sufficient homogeneity. The suspension properties are listed in Table 1.

Table 1: physical properties of suspension

Quantity	Value
Polystyrene density	1050 kg/m^3
Polystyrene radius	60 µm
Mineral oil density	875 kg/m^3
Mineral oil viscosity	0.036 Pa.s
Mineral oil surface tension	0.0285 N/m

The distribution of particles is investigated at various bath size. The wall effects considered as a function of bath width.

The first step is to validate the implemented algorithm. The behavior of suspensions in a rectangular channel using the new algorithm is compared with experimental measurements by Lyon and Leal (1998). They measured the concentration of the particles via Laser-Doppler Velocimetry (LDV). (Lyon and Leal, 1998).

The simulation results using the implemented algorithm in Goma is shown in Figure 7. The particles uniformly distributed throughout the channel initially with a concentration of 0.4. This concentration is used for validation simulation, in order to compare the results with the aforementioned literature. Indeed, it is the separate simulation than the main study and the value used in every section is incorporated into the tables. The

volume fraction exhibits a significant change from the channel wall to the center. The maximum concentration of particles observed at the center.
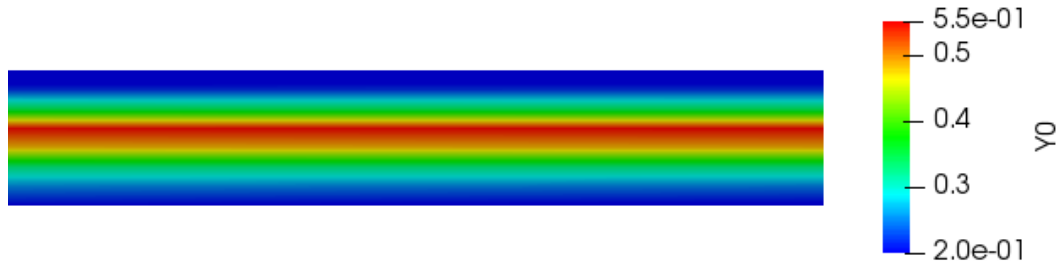

Figure 7: Particle distribution in rectangular channel, initial concentration $\varphi = 0.4$

As shown in Figure 8 the feature of the simulated particle concentration profile is in good agreement with experimental results in the central regions where the wall effect is negligible. The observed difference in the wall can be attributed to the indirect measurements of the volume fraction values with LDV. The experimental measurement of particle concentration near the wall is lower than the actual concentration. The property of LDV called a lower signal to noise ratio caused this reduction. This results in reduction in the probability of measuring particles traverse the probe volume compared to the actual flux of particles. Consequently, the measured particles number per unit time is lower than the actual number, so the lower concentration was reported.
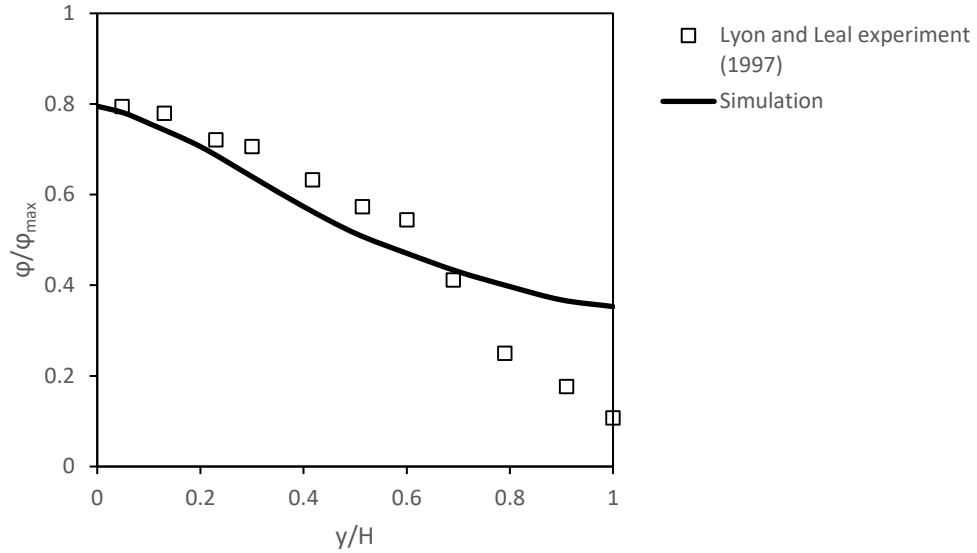
Figure 8: Concentration variation in rectangular channel cross section ($\varphi = 0.4$)

3.4.1 «Mesh Generation»

The numerical simulation in Goma requires a discretization to consist of a large number of elements. The key factor to achieve an accurate result is the mesh quality. The refinement process for capturing the results are more prevalent therefore the refined mesh is applied on 2D geometry such that dense mesh is used near the substrate and a larger mesh for regions far from it. We define symmetry about a centerline and the infinite substrate. A sample mesh used in simulations is illustrated in Figure 9.
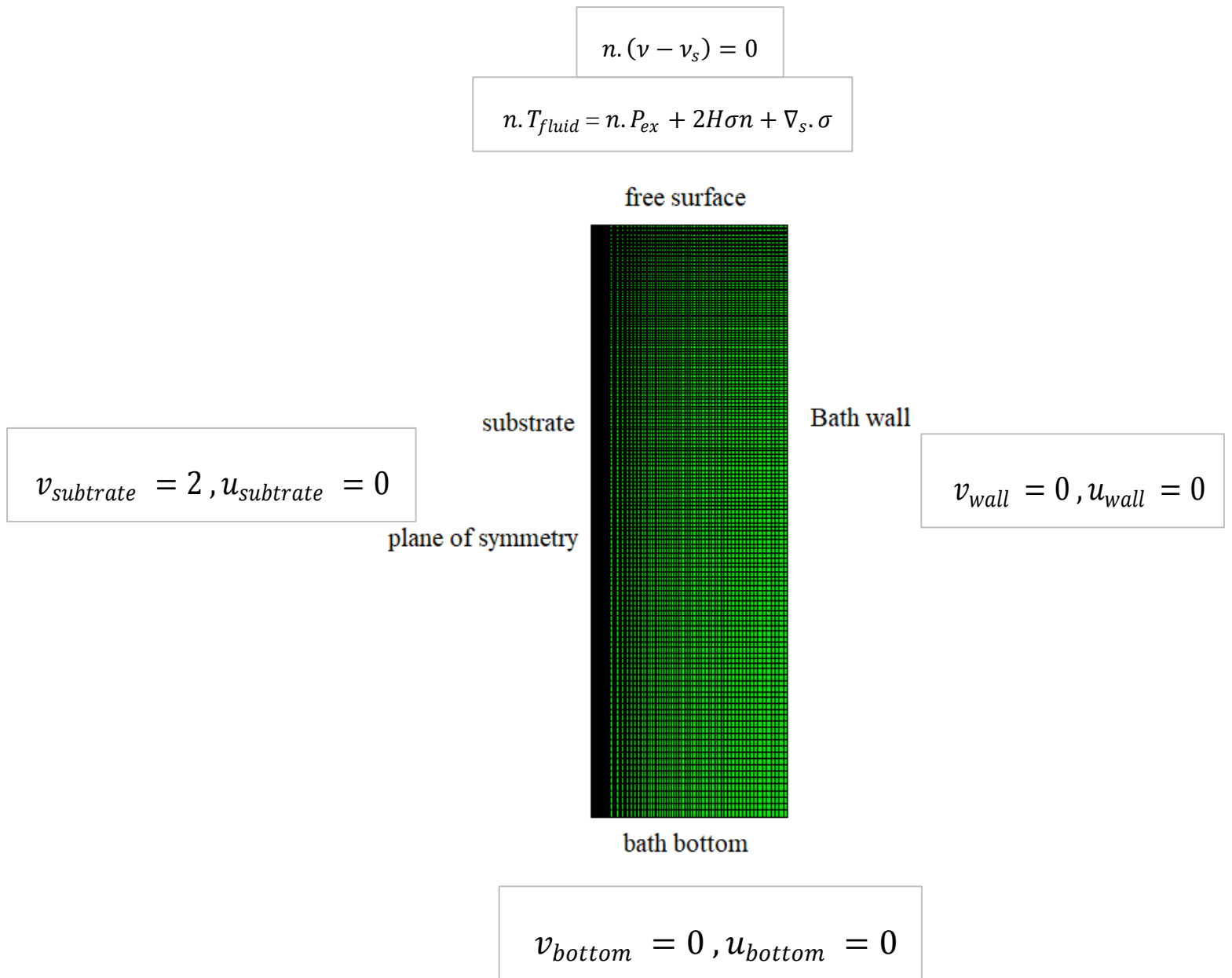
$$n.(v - v_s) = 0$$

$$n.T_{fluid} = n.P_{ex} + 2H\sigma n + \nabla_s.\sigma$$

free surface

substrate

Bath wall

$$v_{subtrate} = 2 , u_{subtrate} = 0$$

$$v_{wall} = 0 , u_{wall} = 0$$

plane of symmetry

bath bottom

$$v_{bottom} = 0 , u_{bottom} = 0$$

Figure 9: Schematic of boundary conditions and refined mesh (not to scale)

Grid size effect on particles distribution is elucidated by a mesh sensitivity analysis. Small cell size, as well as high mesh density, is necessary to acquire accurate film thickness and particles distribution in the coating film. In order to the study the mesh independency and make sure the results are independent of mesh the simulation for different mesh size from coarse to fine mesh is examined. The shape of the free surface is

considered the determining factor for the accuracy of results. The number of elements used in each category is presented in Table 2.

Table 2: Number of elements used in three different meshes

Mesh type	fine	medium	coarse
Number of Elements	27648	14800	13400

Figure 10 shows the shape and location of the free surface for different size of meshes. The plots overlapped each other so the numerical results are independent of the mesh. The negative value shows the reduction of the level of the free surface which was initially located at 0.

The fine mesh results display a smooth transition of flow and concentration changes within the bath, but the computational time is much higher compared to other mesh sizes. The computation simulations time varies based on computation factors such as processor, memory, graphics power and RAM. It also changes by velocity and bath size in which higher withdrawal velocity and bigger bath size increase the simulation time. The computational time with withdrawal speed 2 cm/s and volume fraction of 0.2 on a medium-mesh took 5 hr.

The medium mesh size is chosen for particle distribution within the bath of suspension in order to achieve an acceptable result for simulation. The median size is not only can lessen the computational time but also provide an appropriate solution.
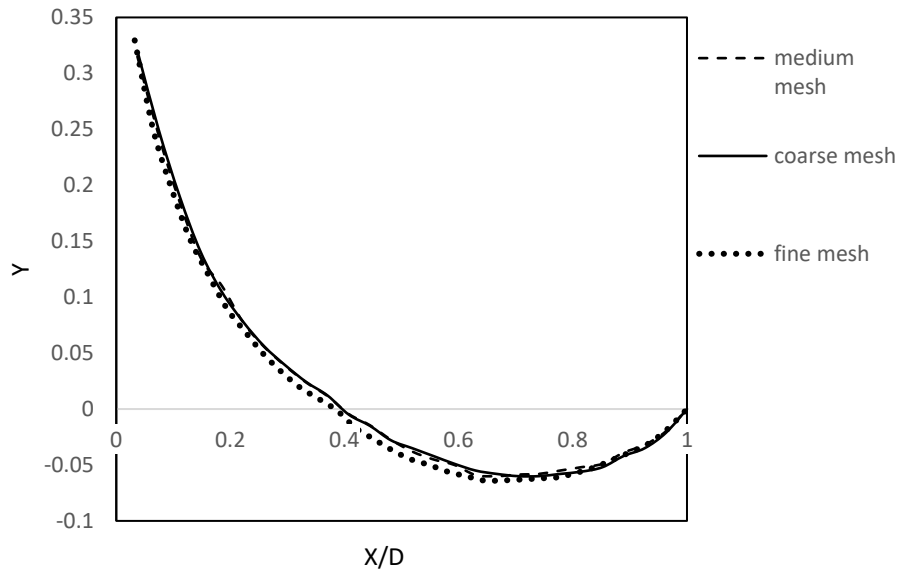
Figure 10: Shape of free surface at three different mesh sizes

The solution procedure for keeping the numerical stability and optimal performance of the processes is by specifying the transient time step in the simulation. Courant number criteria rolls are controlling time step growth which set an upper limit on the time step, regardless of considering the variable time integrator.

The time step limit set by the Courant number limit is calculated as follow:

$$dt_{limit} = Co \min \left| \frac{h_e}{\left\| \hat{U} \right\|_e} \right| \qquad (17)$$

Where e is the element, h_e is the average size of the element, Co is the Courant number, and U is the velocity. Courant number for this study is set to 0.1

The simulation domain for the coating bath is considered as a two-dimensional rectangular domain with a height of 12. The moving substrate was assumed to be centered in the coating bath. The computational times varied based on substrate velocity and the proximity of the initial guess.

Since solving and finding the initial guess for simulation the problem deal with the free surface flow can be a challenging and burdensome task, the Newton correction factor can be utilized with the following method.

Newton correction factor which provides convergent solutions in Newton's method has been changed in order to find a solution for the Newton convergence method. This factor adapts the relaxation choice based on the size of nonlinear residual from the Newton iteration. The Newton correction factor can take a value within a range of $0 < f \leq 1$. The usual Newton correction factor values are 1.0 and applied as the solution converges if not, a percentage of it is applied to the solution. For sensitive problems when the initial guess is too far from the final solution, a value near zero may be applied for the number of initial Newton iterations to help convergence. However, the value of zero is a quite large amount of relaxation, this factor is depending on the problem. An indicator for demonstrating how far the solution is from convergence is the norm of the residual L_∞. The value of the Newton correction factor can be used based on L_∞ on the table

Table 3: The value of the Newton correction factor based on the residual norm

Rang of residual norm	Newton correction factor
$L_\infty > 10^{-3}$	0.1
$10^{-4} < L_\infty \leq 10^{-3}$	0.4
$10^{-6} < L_\infty \leq 10^{-4}$	0.8
$L_\infty \leq 10^{-6}$	1

The relaxation factor through Newton iteration shortens the vector of solution update. Many factors can affect negatively the effective radius of convergence. The poor initial solution, non-analytic constitutive models or boundary conditions, and poor linear solver

performance are among the utmost influential factors to cause the effective radius of convergence of Newton's method to be fairly small or malformed (Schunk et al., 1996).

3.4.2   «Boundary Condition»

For discretization of the simulation domain, well-defined boundary conditions are required. Boundary conditions are defined for the bath wall, bath base, free-surface, and the substrate. After generating the appropriate mesh entity, we have defined side sets and node sets. A node-set includes a group of nodes, apply on Dirichlet boundary conditions in which FEM substitution of the nodal values into the solution vector provides an easy way to use these boundary conditions. A side set includes a group of elements edges or faces.

i)   The boundary condition at the substrate

Withdrawal speed condition is specified for the defined nodes on the substrate. We also defined no slip at the substrate boundary conditions.

$v_{subtrate} = 2 , u_{subtrate} = 0$

ii)   The boundary condition at the bath wall

The velocity component in the direction of x and y is set to zero for bath wall and bath base

$v_{wall} = 0 , u_{wall} = 0$

iii)   The boundary condition at bath base

$v_{bottom} = 0 , u_{bottom} = 0$

iv)   The boundary condition at the free surface

The distinguishing conditions have been applied to locate the free surface. The kinematic condition provided in Goma in conjunction with Capillary was set along

the free surface. The applied kinematic boundary as a condition on the mesh motion equations enforces no mass loss or mass gain of fluid through a free boundary by deforming the mesh. The functional form of kinematic boundary condition defined by the following equation.

$$n.(v - v_s) = 0 \tag{18}$$

Where n is the unit normal vector to the free surface and v represents the velocity of fluid and v_s is the surface velocity (Sackinger et al., 1996).

The existence of surface tension related forces is one of the predominant characteristics of the free surface. A capillary condition specifies the capillary forces i.e. surface tension applied to the momentum equation on the free surface. The forces applied on free surface set by the following equation:

$$n.T_{fluid} = n.P_{ex} + 2H\sigma n + \nabla_s.\sigma \tag{19}$$

n is the outward normal to the surface, fluid stress tensor is shown by T, P_{ex} represents the external applied pressure and H is the curvature and ∇_s denotes the surface divergence operator.

3.4.3 «Validation of simulation results with experimental data»

In order to validate the simulation results, the thickness of the deposited film was compared with the experimental results of previous work by Javidi et al (2015). The measurement had been carried out at substrate velocity 0.05 cm/s and particle concentration 0.2 vol%. As shown in Figure 12, the higher part of the substrate assumes to be 0 cm and the final part of the substrate being withdrawn as 6.5 cm. It can be observed that gravity forces cause the thickness of the film in the higher area to decrease gradually. The numerical result is in good agreement with the experimental data (Javidi and Hrymak, 2016).

The initial mesh is highly refined toward the moving contact line because the elements near the contact line will be subject to distortion. So small elements minimize the effect of distortion. In the following, it is best to remesh the deformed mesh when it has lost its original integrity. The prepared mesh close to the contact line is shown in Figure 11.
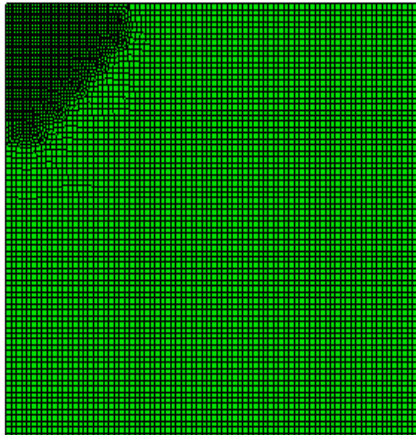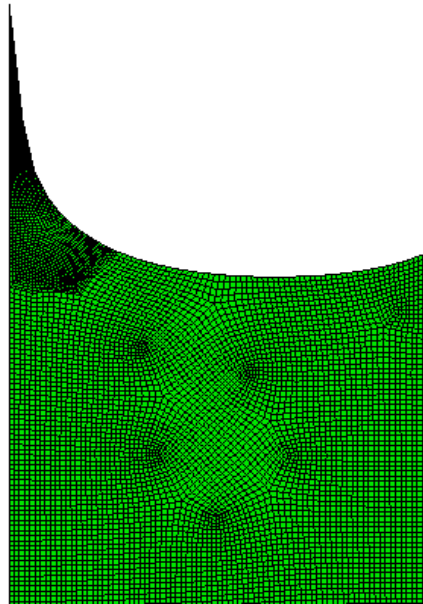
a)   b)

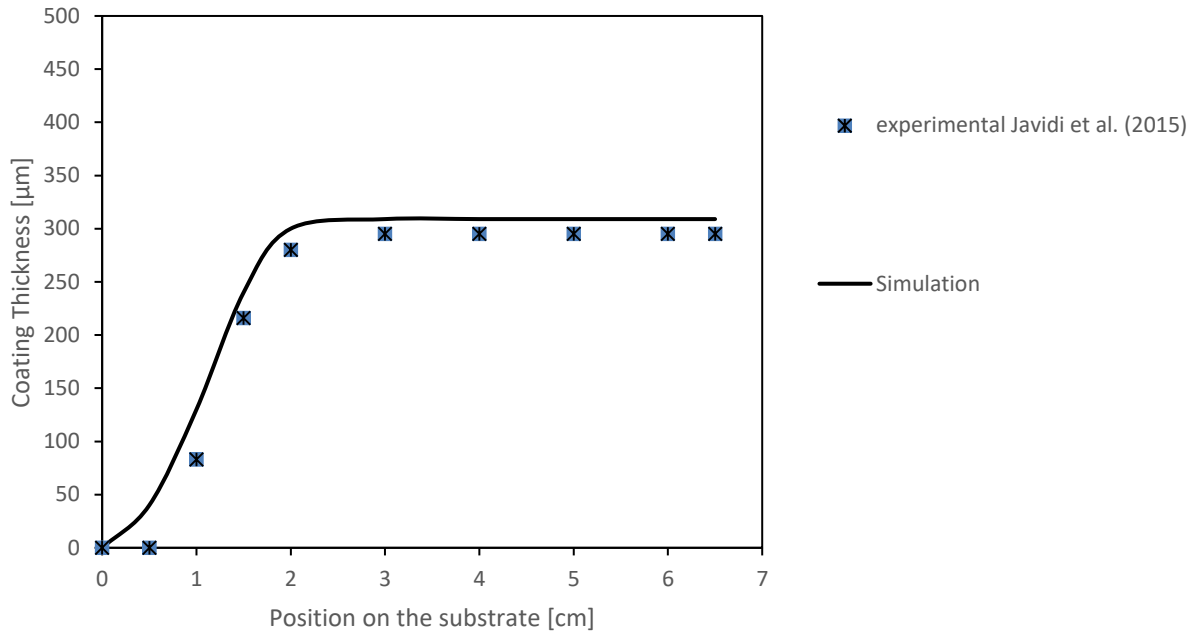**Figure 11**: mesh used in coating thickness measurement a) original mesh, b) the mesh of the deformed domain

Figure 12: The comparison profile of film thickness measurement at numerical prediction with experimental data

3.4.4 «Solution Approach»

As stated earlier, momentum, continuity, and interpolated velocity gradient equations are solved by the FEM with diffusive flux model as a constitutive equation for particle migration. Newton's method is applied to solve non-linear algebraic equations. In this method, the problem converges quadratically when initial guess is near the solution. In order to yield the solution, some steps are needed to be done because the problem is highly nonlinear.

i)   The primary step for solving the equations in this study was performing a simulation on a fixed grid. Therefore, the kinematic and capillary condition was turned off from the boundary condition and the simulation was run with the normal velocity and no tangential velocity was specified. Under this circumstance, the boundaries become shear stress-free with their respect to the liquid. The normal velocity component is relative to the motion of the

underlying mesh. The solution for the first step was used as an initial guess for the next step.

ii)   In the second step, normal velocity condition had been replaced with the kinematic and capillary boundary conditions. As a result, these boundaries allow the free surface to be released.

(Schunk et al., 2013)

3.5 «Results and discussion»

For suspension prepared with a Newtonian carrier fluid, the simulation has been carried out and distribution of particles within the coating film is elucidated. The particle concentration varies across the flow domain and viscosity of the suspension is computed based on the volume fraction of the particles at each point, which is implemented in the equations.

The general characteristics of the dip coating process, deformation of free surface shape and level, and velocity magnitude are presented. The effects of particle migration on the flow field, wall proximity, particle concentration, and particles radius are reported.

In section 3.5.1, in order to investigate the wall effect on particle distribution, the analysis of particle concentration changes throughout the coating film with the variation of the substrate to wall distance is presented.

In section 3.5.2, the effect of changing the particle concentration is presented and section 3.5.3, the results of different particle radius and its effect on concentration distribution is elucidated. In section 3.5.4. the withdrawal speed is varied and the effects on the particle distribution presented.

The level of free surface gradually declined while the substrate is pulled out of the bath. Figure 13 illustrates the stagnation point and velocity distribution throughout the region near the free surface. It can be observed that the flow adjacent to the substrate move upward with the same velocity as the substrate. While the substrate movement generates

a deformation of the free surface which is subject to resistance by the surface tension. The interplay of these forces is known as the capillary number. On the other hand, velocity decreases from substrate until it becomes zero at the free surface, known as stagnation point while at a region far from the substrate, in the recirculation flow region, gravity causes the fluid to return into the bath.
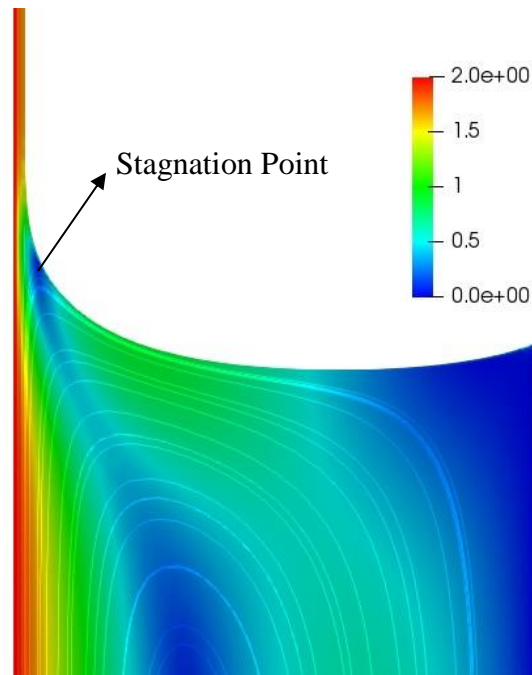

Figure 13: Velocity magnitude and streamlines in the dip coating process at the substrate velocity 2 cm/s

Figure 14 provides the distribution of velocity within the liquid bath in width direction, which is determining the stream circulation throughout the bath. The y and x correspond with the vertical direction and horizontal direction, respectively.
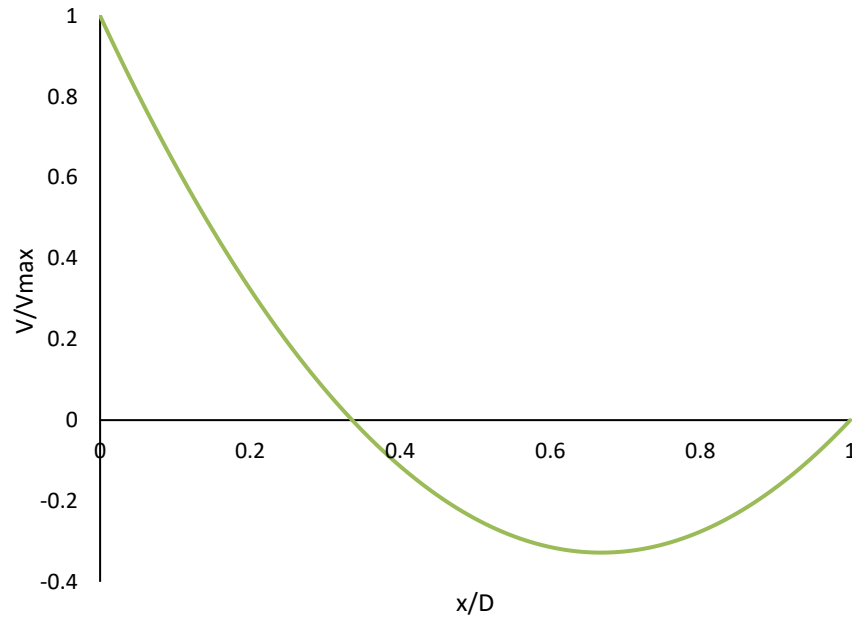
Figure 14: Vertical velocity of flow in the dip coating process at the center of bath

Because the capillary number plays a significant role in the dip coating process, numerical analysis has been performed at the constant capillary number. The plots of free surface at lower and higher viscosity attributed respectively to the higher and lower velocity, are illustrated in Figure 15. The shape of the surface does not change when the capillary number remains constant. Assuming that the initial level of the free surface is located at 0 cm.
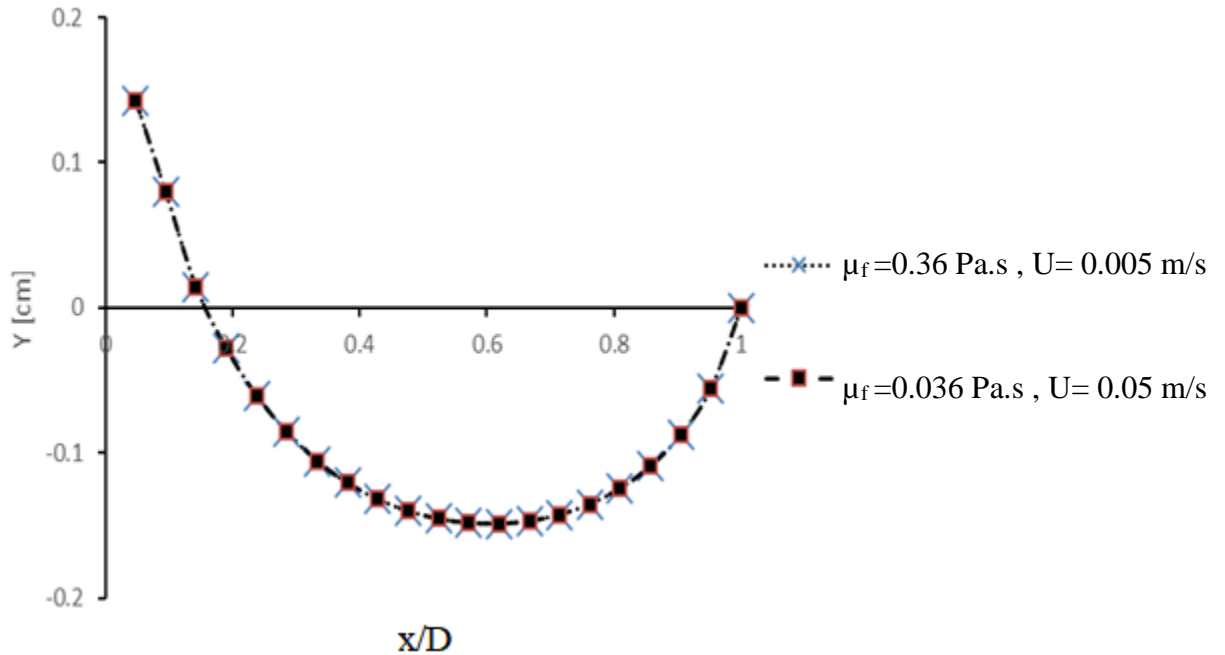
Figure 15: Free-surface displacement at two different conditions at *Ca*= 0.12

In suspension flows, complex phenomena arise which is the result of shear-induced migration and interaction between particles. Moreover, during the dip coating process, the hydrodynamics of the bath liquid affects the particle distribution while the substrate is being withdrawn. Indeed, particle distribution undergoes a fluctuation because of shear rate variation. That leads to the accumulation of particles either in the corners or the center part where the shear rate vanishes and moving away from walls and free surface as well. As the process goes on, the preliminary uniform dispersion converts to the non-uniform alignments state.

3.5.1   Analysis of Wall Effect

In order to examine the wall effect on concentration distribution in the dip coating process, simulation analysis has been performed at three different substrates to wall

distances. The gradients in volume fraction of particles and the dependency of suspension rheology on concentration alter the flow characteristics from Newtonian fluids.

Consequently, particles tend to accumulate at the center part of the bath where there is a relatively low shear rate. The free surface induces particle depletion adjacent to the withdrawing surface. It shows that particles concentration undergoes the uneven distribution in the presence of the free surface.

Furthermore, the close proximity of the wall affects the concentration profile in the dip coating process. The dynamic of the flow domain within the bath can clarify the wall effect on the concentration gradient. As discussed by Javidi et al. (2015), the stagnation point is located closer to the substrate in case of the smaller width of the bath. Thus, the circulation of suspension flow occurs in the more confined region. While the flow moves with opposite direction of withdrawal velocity on the right side of the stagnation point result in creating a zero-shear rate zone.

In this section, an analysis of the important observed features related to particle migration in the coating film is presented for the different substrate to wall distances. The goal is to understand how the proximity of the bath wall affects the particle distribution in the coating film. The model represented in this work includes the particle concentration change with particle volume fractions of 0.2. The value of parameters used in this examination are presented in Table 4.

3.5.1.1　Shear rate

Furthermore, the measurement of free surface shape is performed in order to investigate the bath geometry effect on the final film. Figure 16 exhibits the change of interface as the substrate to wall distance is altered.　As mentioned in literature, in the confined liquid bath, the meniscus has a more curvature shape than in an unconfined bath (Kim and Nam, 2017). Curvature increase affects the capillarity and therefore adjusts the force balance in the dynamic meniscus region. (Kim and Nam, 2017). As a consequence, the film

thickness will decrease with decreasing the size of the bath (Javidi and Hrymak, 2015). The other results would impact on the transition path of particles entraining into the film.

Table 4: The parameters used for the analysis of wall effect

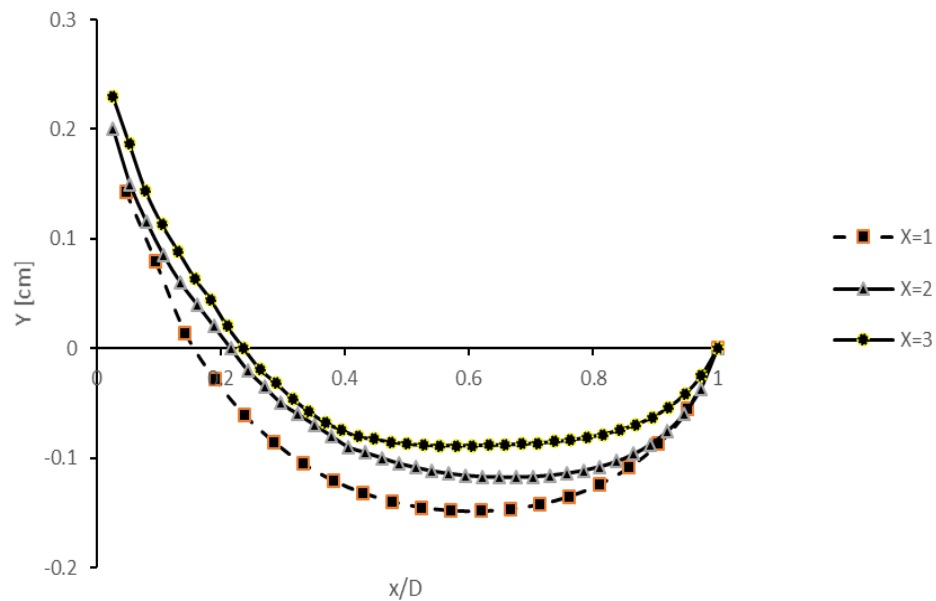| **Bath width**	0.01 m	0.02 m	0.03 m
Substrate velocity	0.02 m/s	0.02 m/s	0.02 m/s
Particle volume fraction	0.2	0.2	0.2
Particle radius	60 µm	60 µm	60 µm
D_φ	1.476×10^{-9}	1.476×10^{-9}	1.476×10^{-9}
D_μ	2.232×10^{-9}	2.232×10^{-9}	2.232×10^{-9}

Figure 16: Free surface for different bath geometry

As shown in Figure 16, as the distance between the substrate and bath wall decreases then there is higher deformation of the free interface. In the region of high free surface deformation, shear rates increase compared to other regions in the bath. Figure 17 depicts the variation of the second invariant of the shear rate in the magnified meniscus region. The gradient of shear leads to the particle migration which will be laid out subsequently. The zero or extremely low shear rate zone below the interface is also notable. The second invariant of shear rate remains almost monotonic above the meniscus into the constant film thickness region.
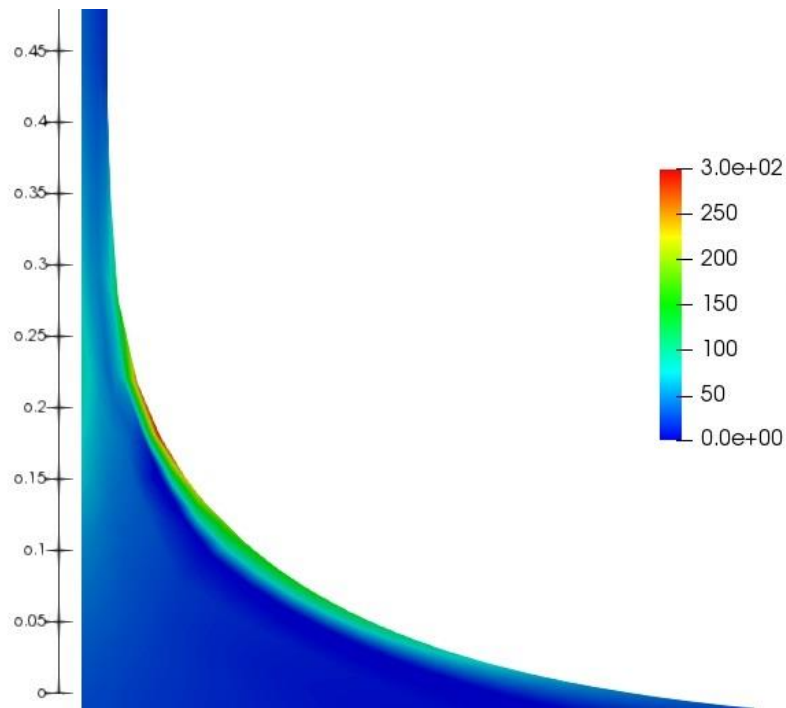

Figure 17: Second invariant of shear rate in bath width=2 cm from GOMA simulation

3.5.1.2   Particle concentration and velocity

The particle concentration field near the free surface and coating film are shown in Figure 18-20 for different baths. There are regions of high and low particle concentration. It

should be noted that in this figure and the subsequent ones, the Y-axis in the vertical from shows the initial level of the free surface which is located at 0 cm.

As shown in Figure 18-20, the variation in concentration throughout the coating film is more pronounced in the smaller substrate to bath wall distance and shows the more evenly distributed of particles when the substrate to bath wall distance increases. Also, it can be seen that the particles accumulated in the region where the flow is returning to the bath and where the shear rate is very small. The accumulated particles did not succeed to entrain into the final film and are returned to the bath. The recirculation region has higher concentration values than the suspension, and then the suspension with high concentration is convected to the top height of the coating film.
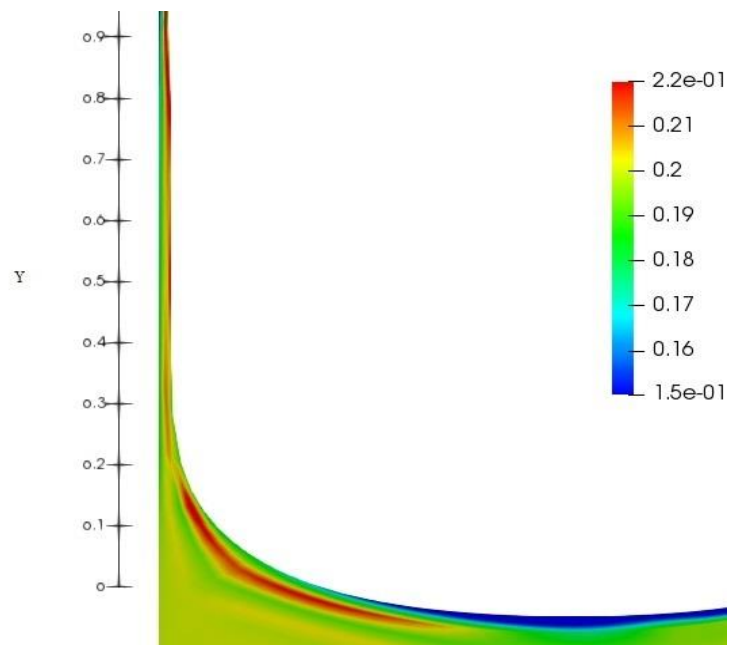

Figure 18: The concentration field evolution in the film thickness and meniscus region in bath width =1 cm
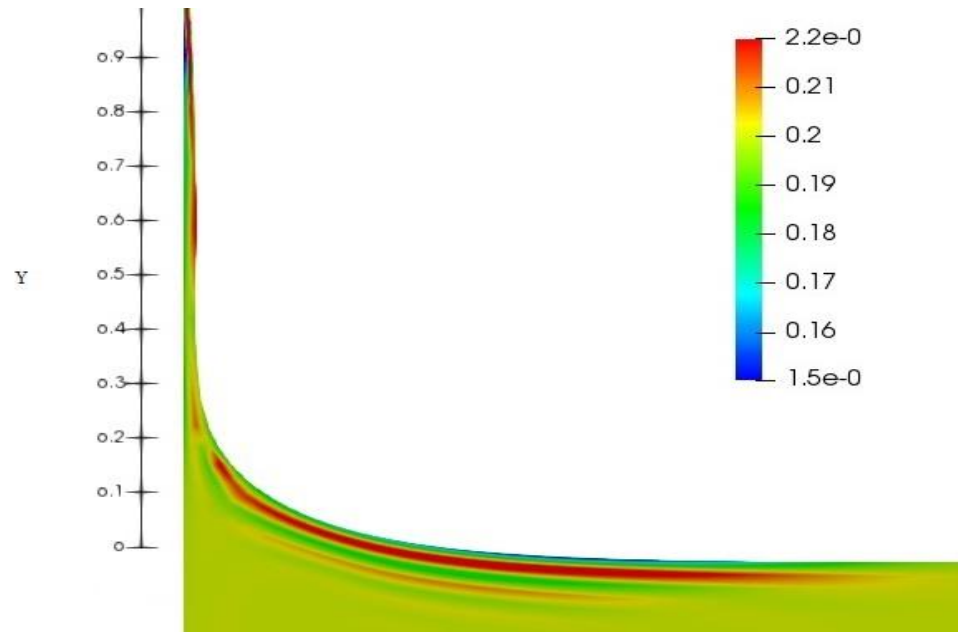
Figure 19: The concentration field evolution in the film thickness and meniscus region in bath width =2 cm
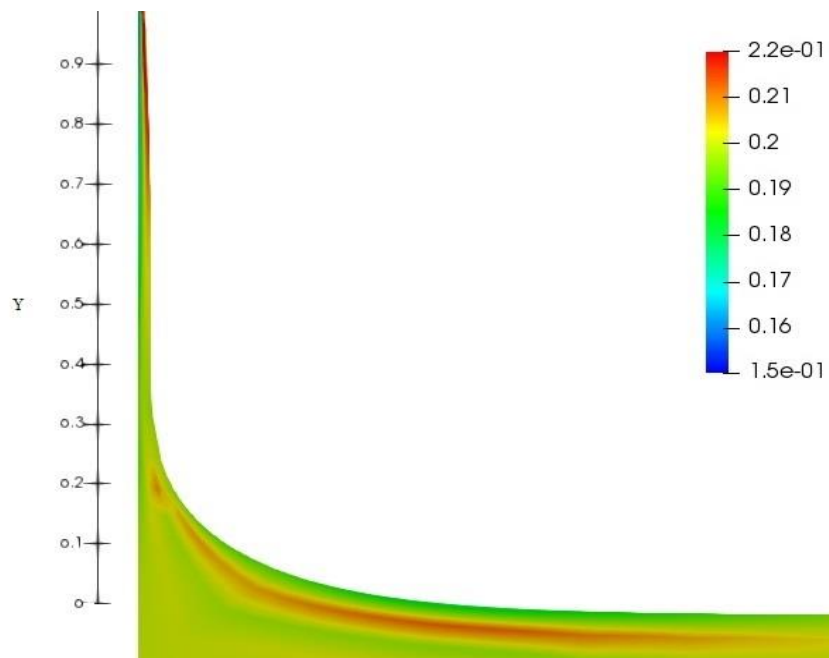

Figure 20: The concentration field evolution in the film thickness and meniscus region in the bath width= 3cm

Flow dynamic in the meniscus part is a combination of drag flow of the substrate upward moving and free surface effects. The main characteristic of this flow is the presence of stagnation point in which the streamline ending at this point defines the shear flow region and recirculation region. The backflow generates a negative velocity and leads to a zero-shear rate zone.

The flow close to the substrate is rectilinear and drag force drives particles into the film. Capillary force exerts normal to the interface and increases with deformation of the interface. (Colosqui et al., 2013). So, there is a combination of deformation of interface and viscous drag forces in this area.

Furthermore, the vertical velocity is dominant along the entrainment region. So, the vertical velocity change accompanied by the concentration change are plotted in detail (Figure 21-25) at different heights starting from bath surface to the top part of the coating film. At the stagnation point, the vertical speed reaches its minimum value.

Figure 21(a) shows the flow velocity at the recirculation zone across the meniscus. Starting from the substrate towards the interface, velocity decreases from its maximum at the substrate until it becomes zero at recirculation area, the corresponding component of velocity gradient decreases as a result. Afterward, velocity reverses its direction and then increases in magnitude. So, the corresponding component of the velocity gradient increases.

Firstly, this trend in velocity gradient resulting in the creation of area which the second invariant of shear rate is zero (Figure 18).

Secondly, the shear gradients cause the particles to migrate which leads to concentration variation across the meniscus. Figure 21(b) shows the concentration profile. Particles migrate away from the moving substrate and also near the interface where the shear rate is high. The peaks in concentration plot correspond to near zero shear rate zones. At the interface, the particle concentration in the bath (X=1) decreases to 0.18 while it decreases to 0.19 in the bath (X=3). The more particle moves away from the high shear rate zone,

the more particle piling up in lower or zero-shear rate zone is. Therefore, the differences in deformation of interface and shear rate in the baths with various sizes lead to the differentiation in particle concentration.
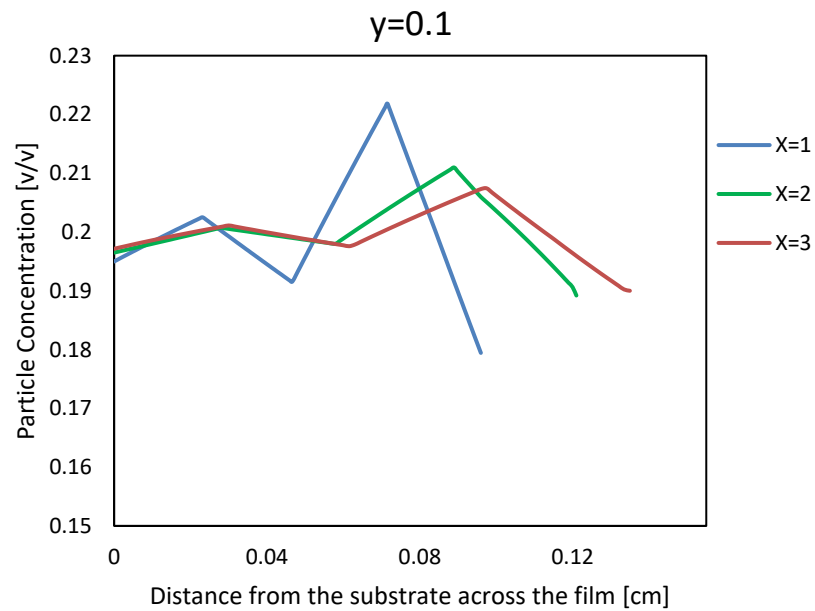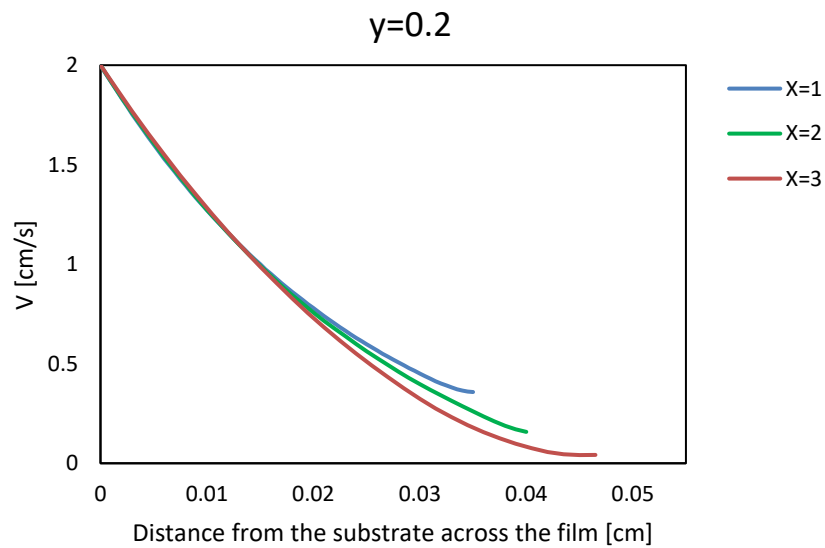
a)
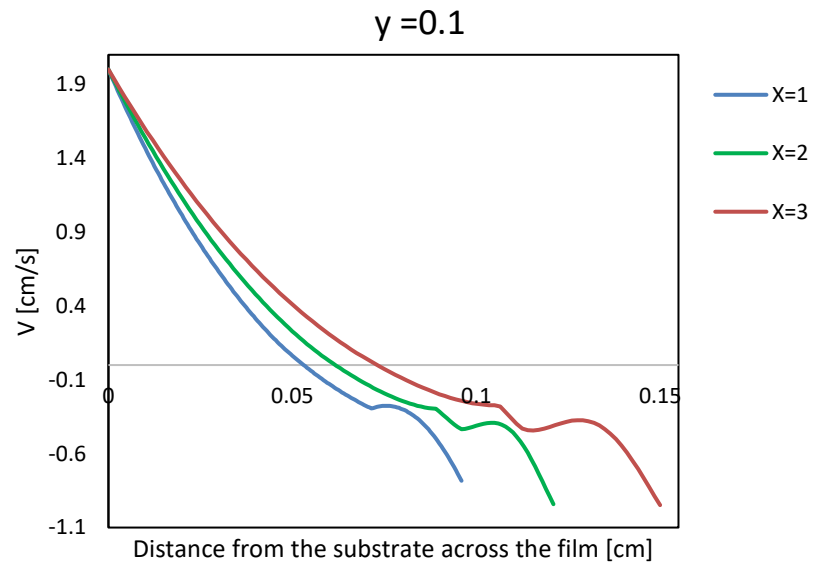
b)

Figure 21: a) Vertical velocity component and b) Particle concentration distribution at the y=0.1 at different baths

Moving up to the area slightly above the stagnation point, vertical velocity drops to nearly zero, while it shows the slow decrease as the substrate to wall distance increases. The concentration at the bath (X=3 cm) remains relatively at the initial concentration. The particles in this area belong to those who pass the recirculation zone and entrain into the coating film. The variation in shear rate causes the particles to migrate and accumulate at the center. Figure 22 compares the velocity and particle concentration across the coating film in this area.
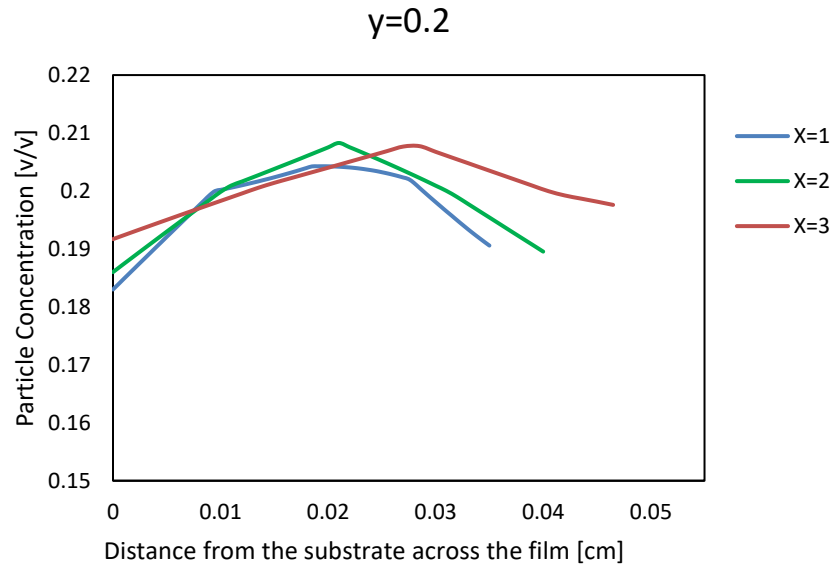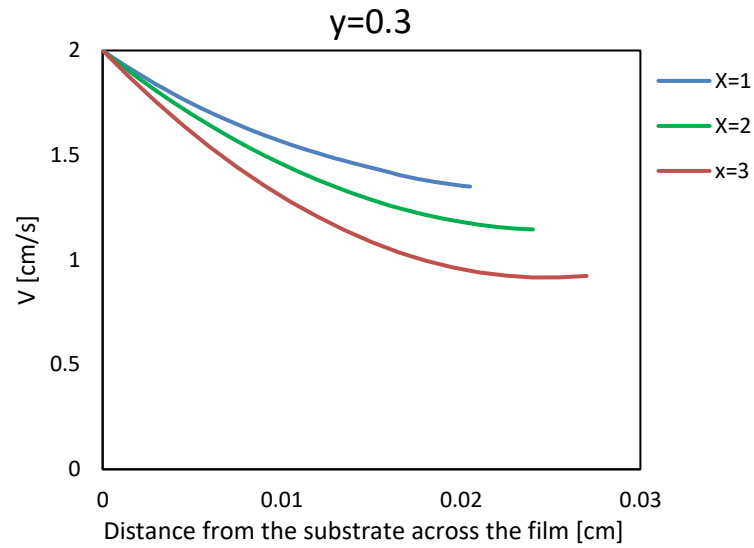
a)

b)

Figure 22: a) Vertical velocity component and b) Particle concentration distribution at the y=0.2 at different baths

Advancing into the coating film region, drag flow dominates the flow field and the effect of the interface deformation diminishes gradually. Drag flow effect causes the variation in particle concentration from here upward to the top of the coating film.

Particle concentration in the bath (X=1 cm) remains higher than the average concentration whereas the particles distribute almost evenly across the film in the bath (X=3 cm). Figure 23 compares the velocity and particle concentration across the coating film in this area. It is also notable that the coating film thickness becomes thinner as it climbs. Velocity changes 32% in bath X=1 cm and 42%, 54% in bath X=2 and 3 cm respectively which demonstrate the velocity stay higher throughout the coating film as it is processed in the thinner film.
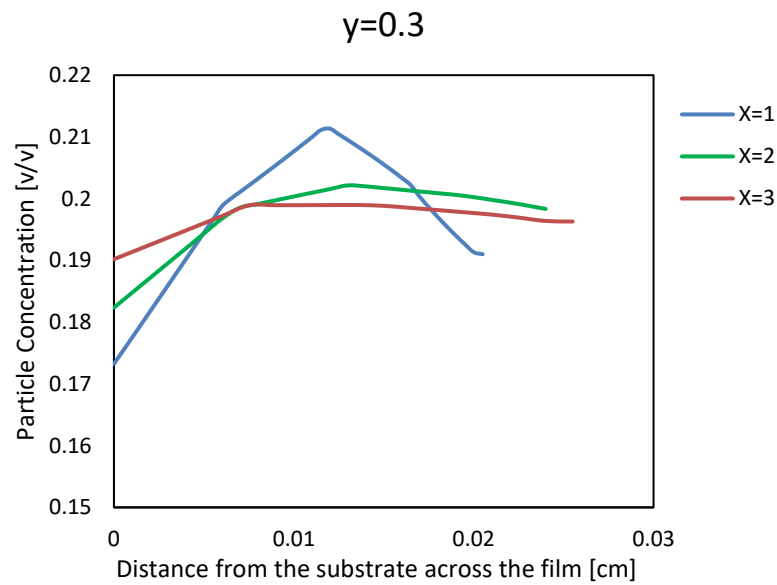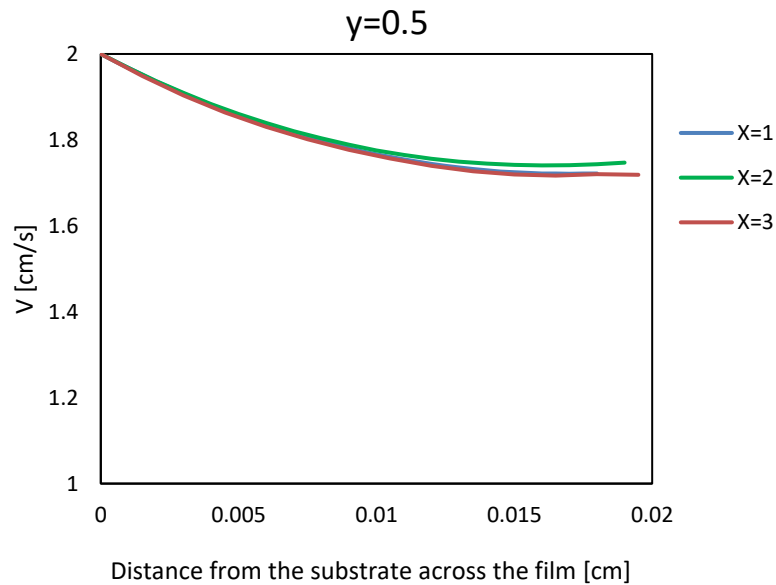
a)

b)

Figure 23: a) Vertical velocity component and b) Particle concentration distribution at the y=0.3 at different baths

Figure 24 and Figure 25 shows the velocity and particle concentration across the coating film in the coating film area at two top heights. The drag flow is responsible to drive particles into the coating film in this area. Velocity plots in all cases have overlapped each other and show a slight decrease across the coating film. This trends in velocity shows that the shear rate has a weak effect in the developed coating film. It is also observed that higher concentration at the surface of the coated film that results from particle moving away from the moving substrate.
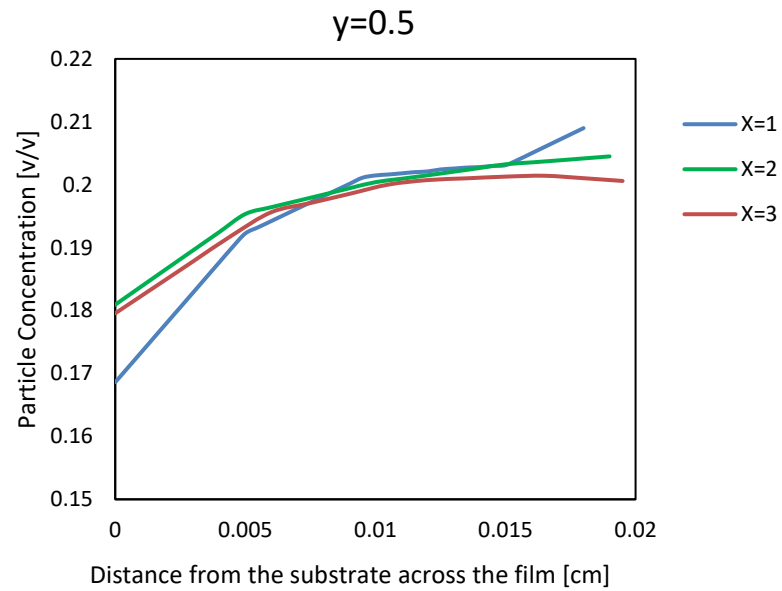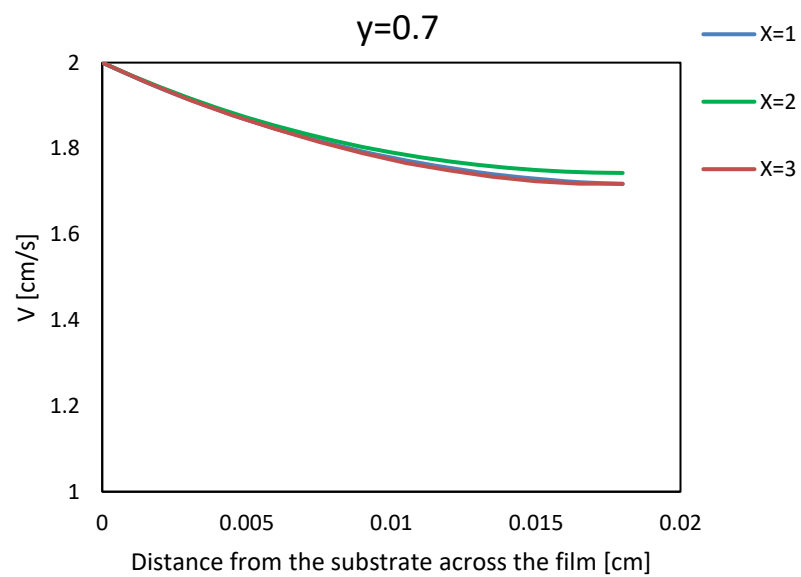
a)

b)

Figure 24: a) Vertical velocity component and b) Particle concentration distribution at the y=0.5 at different baths

a)

b)

y=0.7
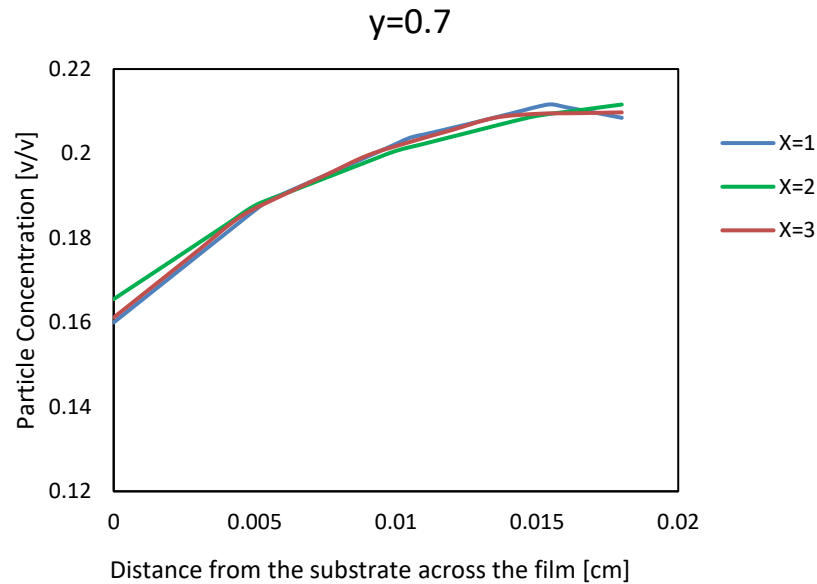
Figure 25: a) Vertical velocity component and b) Particle concentration distribution at the y=0.7 at different baths

The complex phenomena in suspension flow happen as results of particle-particle interactions which cause the shear-induced migration and particle arrangement based on flow kinematics. At the coating film region, above the meniscus, the flow is purely drag flow, the shear rate is almost constant so there is no or weak migration owing to shear rate gradients. Strong migration of particles from the substrate toward the interior and outer part of the film occurs, accordingly, the concentration decreases.

3.5.2   Analysis of Concentration Effect

In order to examine the concentration distribution in the dip coating process, simulation analysis has been performed at three different concentrations.

In this section, an analysis of the important observed features related to particle migration in the coating film is presented for different concentrations. Other parameters remain the same. The goal is to understand the effects of concentration on the particle distribution in the coating film. The value of parameters used in this examination are presented in Tables 5.

Table 5: The parameters used for the analysis of particle concentration

Bath width	0.02 m	0.02 m	0.02m
Substrate velocity	0.02 m/s	0.02 m/s	0.02 m/s
Particle volume fraction	0.1 [v/v]	0.2[v/v]	0.3 [v/v]
Particle radius	60 µm	60 µm	60 µm
D_φ	1.476×10^{-9}	1.476×10^{-9}	1.476×10^{-9}
D_μ	2.232×10^{-9}	2.232×10^{-9}	2.232×10^{-9}

The particle concentration field near the free surface and coating film are shown in Figure 26 for lower concentration. There are regions of high and low particle concentration. As shown in Figure 27, the variation in concentration throughout the coating film is more pronounced in higher concentration and demonstrate the more evenly distributed of particles in the 0.1 of particle concentration. The vertical velocity accompanied by the concentration change across the coating film are plotted in Figure 28. The results show that as the concentration increases resulted in an increase in the particle depletion from the substrate. The greater velocity gradient is also predicted at a higher concentration which leads to an increase in local shear rate near the substrate region.

Figure 26: The concentration field evolution in the film thickness at a concentration of

0.1

Figure 27: The concentration field evolution in the film thickness at a concentration of

0.3

a)

b)

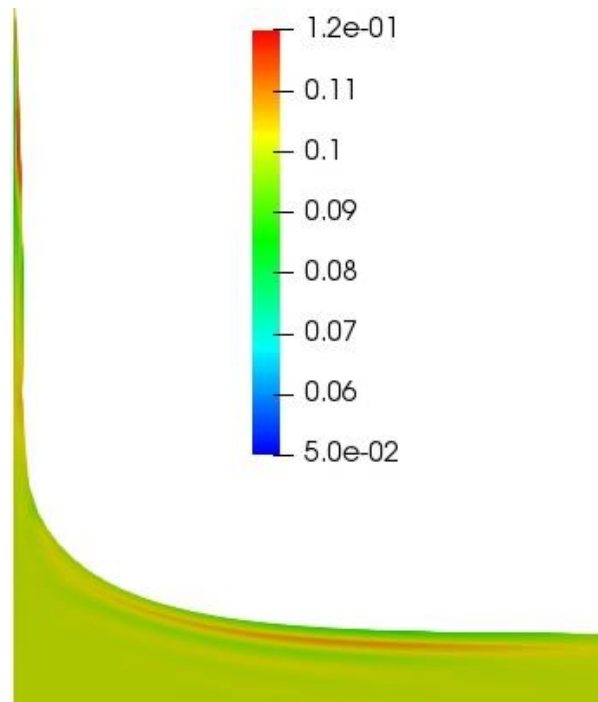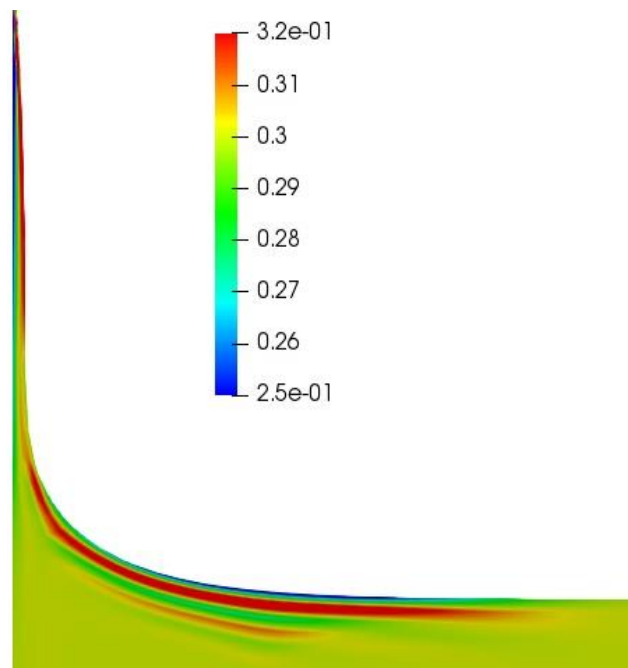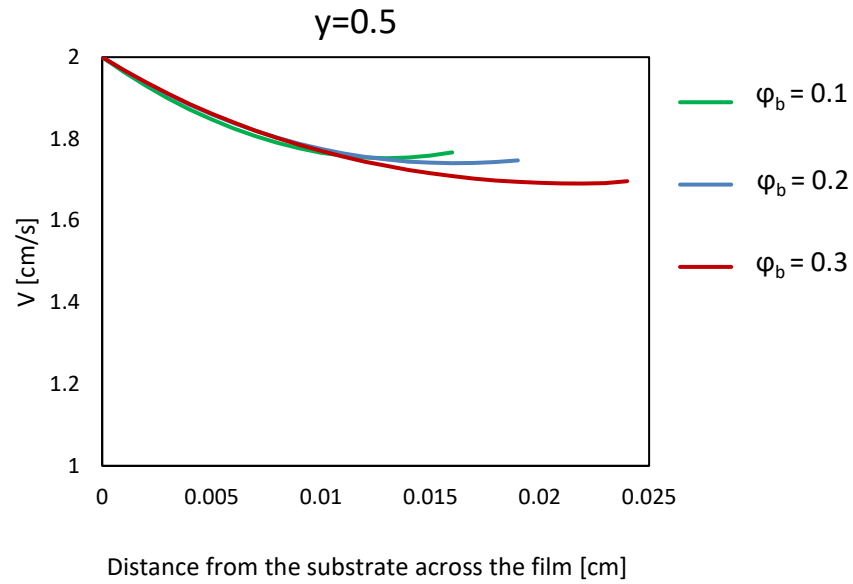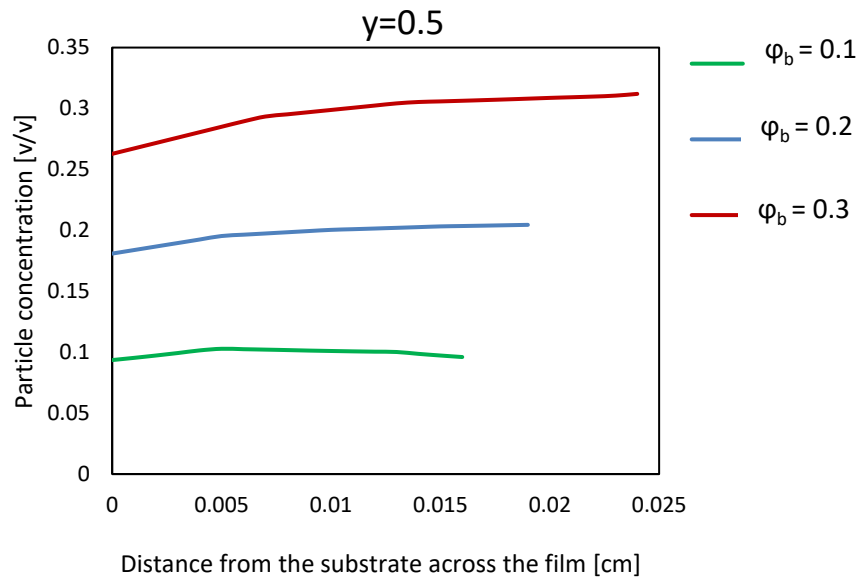**Figure 28**: a) Vertical velocity component and b) Particle concentration distribution at the y=0.5 at three different concentrations

3.5.3   Analysis of Particle Radius Effect

In this section, an analysis of the observed features related to particle migration in the coating film is presented for different particle radii. Other parameters remain the same. The value of the parameters used in this examination are presented in Table 6. Note that changing the particle radius, in fact, result in the variation of the diffusion coefficients which is calculated accordingly.

Table 6: The parameters used for the analysis of particle radius

Bath width	0.02 m	0.02 m
Substrate velocity	0.02 m/s	0.02 m/s
Particle volume fraction	0.2 [v/v]	0.2 [v/v]
Particle radius	60 µm	30 µm
D_φ	1.476×10^{-9}	3.69×10^{-10}
D_μ	2.232×10^{-9}	5.58×10^{-10}

The particle concentration field near the free surface and coating film are shown in Figure 29 for particle radius of 30 µm. The vertical velocity accompanied by the concentration change across the coating film are plotted in Figure 30. Although the curves show uniform concentration across the film, there is a difference between the two curves. The curve of suspension with the smaller particle appears to be flatter than the curve of suspension with the larger particle. It is observed that the larger the value of the particle radius the more particles have migrated away from the moving substrate and the particle concentration at the center does not change much.
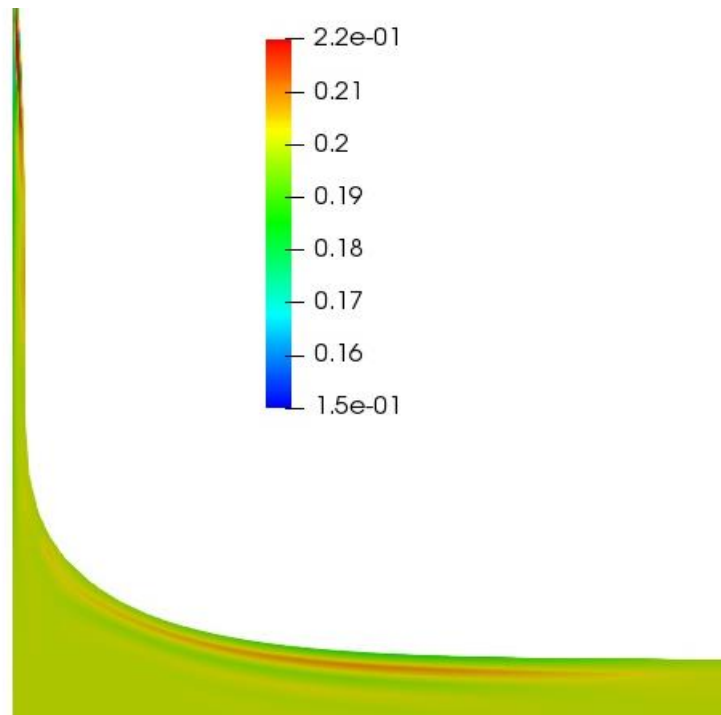
Figure 29: The concentration field evolution in the film thickness with particles radius of 30 μm

a)
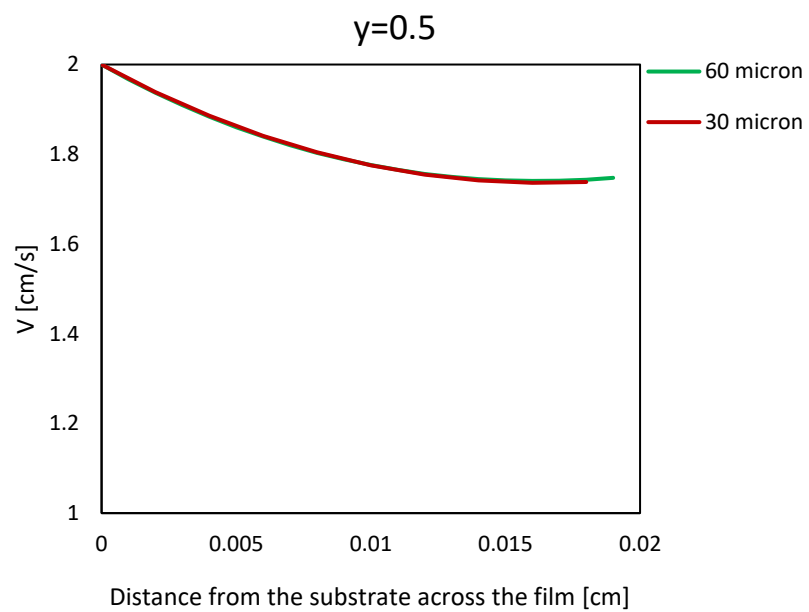
b)
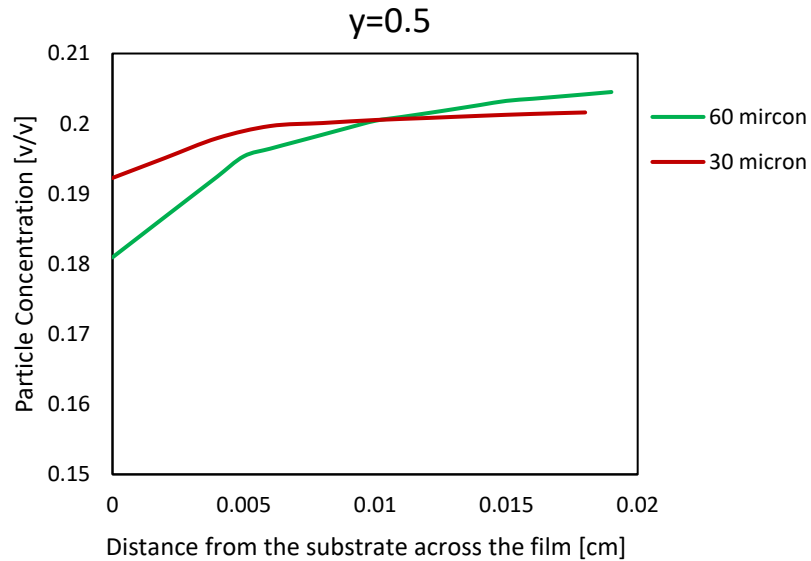
Figure 30: Vertical velocity component and b) Particle concentration distribution at the y=0.5 for different particle radii

3.5.4　Analysis of Velocity Effect

In this section, an analysis of the observed features related to particle migration in the coating film is presented for three different substrate withdrawal velocities. Other parameters remain the same. The value of the parameters used in this examination are presented in Table 7. The goal is to understand the effects of velocity on the particle distribution in the coating film. The vertical velocity accompanied by the concentration change across the coating film are plotted in Figure 31.

It is seen that the particle distribution throughout the film is almost the same except the value of film thickness. The coating film thickness is increased by increasing the withdrawal speed. A layer of high concentration is formed at the outer side of the coating

film while adjacent the substrate the concentration is lower than the bulk concentration. The high concentration at the outer part changes slightly with the speed.

Table 7: The parameters used for the analysis of substrate velocity

| Bath width	0.02 m	0.02 m	0.02m
Substrate velocity	**0.02 m/s**	**0.03 m/s**	**0.04 m/s**
Particle volume fraction	0.2	0.2	0.2
Particle radius	60 µm	60 µm	60 µm
D_φ	1.476×10^{-9}	1.476×10^{-9}	1.476×10^{-9}
D_μ	2.232×10^{-9}	2.232×10^{-9}	2.232×10^{-9}

a)
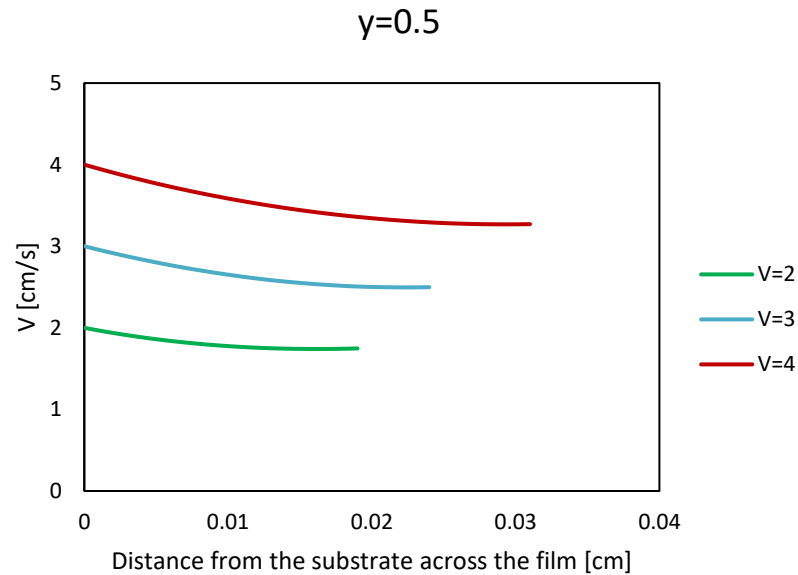
b)
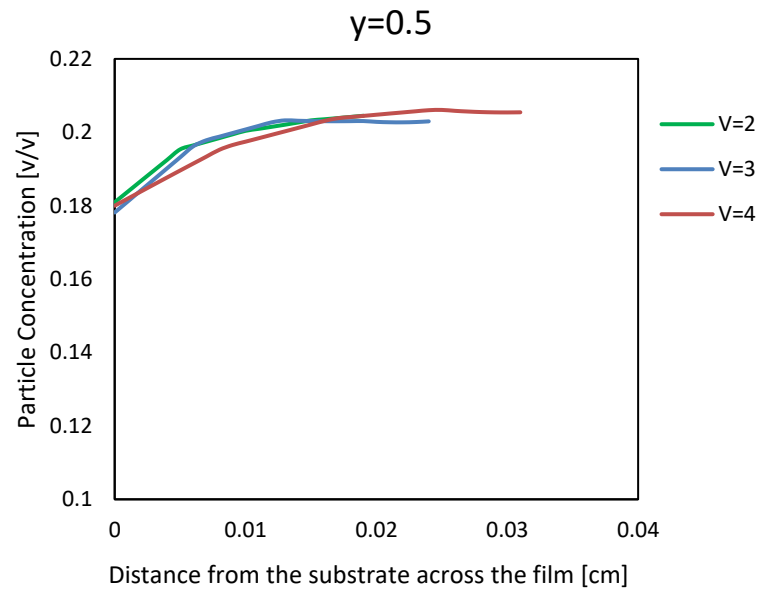
Figure 31: Vertical velocity component and b) Particle concentration distribution at the y=0.5 for different velocities

Chapter 4

4   « Concluding remarks and summary»

4.1   « Conclusions »

In this study, the two-dimensional flow of a dip coating process was examined. Withdrawal of infinite substrate throughout the concentrated suspension was considered for simulation investigation. The numerical simulation for suspension flow in dip coating was developed in Goma finite element software. The neutrally buoyant suspension considered as a Newtonian fluid with a concentration-dependent viscosity. An employed continuum constitutive equation was based on the diffusive flux model in two-dimensional flow.

The main focus of this study was the investigation of wall proximity on the distribution of particles in coating film in the dip coating process. Several parameters were taken into consideration in order to elaborate their effect as well. These parameters include the wall proximity, particle concentration, particle radius, and withdrawal speed.

The simulation results showed the particle migration throughout the meniscus and coating film. The gradients of shear cause the particles migrate which leads to concentration variation. There is an accumulation of particles where the shear rate is relatively small. This refers to the area in the recirculation zone.

The simulation results showed that during the dip coating process, the level of free surface gradually declined while the substrate is pulling out of the bath. The shape of the meniscus is affected by the size of bath width in which the smaller the width of the bath the more curvature of the meniscus. To put this in perspective, the alteration in meniscus shape affect the film thickness and deposition of particles on the substrate.

For wall proximity, the model prediction reveals the stronger migration of particles into the film as the bath size get smaller. The more particle moves away from the interface the more particle piling up in zero-shear rate zone is. Therefore, the differences in

deformation of interface and shear rate of the baths with various size lead to the differentiation in concentration.

Furthermore, model predictions of different concentrations illustrate the variation in concentration throughout the coating film. The effect of particle migration is more pronounced in higher concentration and the particles are more evenly distributed in the lower value of particle concentration.

Additionally, the results demonstrate that the smaller particle appears to have more uniform distribution than the larger particle. It is observed that the larger the value of the particle radius the more particles have migrated away from the moving substrate. The film thickness in suspension with the larger particle is slightly greater than the suspension with smaller particles.

It is found that there are minor particle distribution variations throughout the film at different substrate velocities in the range examined. However, the coating film thickness is increased by increasing the withdrawal speed. A layer of high concentration is formed at the outer side of the coating film while adjacent the substrate the concentration is lower than the bulk concentration. The high concentration at the outer part changes slightly with the speed.

The data can be used to predict how the changing of the operating parameters and the properties of the suspension can affect the particle distribution in the coating film.

In order to produce a coating film with a uniform distribution of particles, the following points can be made. Overall, smaller particle radius, lower particle concentration, lower substrate velocity and most importantly the larger the bath to substrate distance result in more uniform particle distribution in the film.

4.2 «Future Work»

After accomplishing the simulation related to the dip coating process; some investigation is recommended for the future.

- While in current work the Newtonian fluid is considered for further research, it can be extended to studying the non-Newtonian fluid and revealing the viscoelastic behavior of these flow as it covered more coating fluids used in industry.

- An experimental study is recommended using Nuclear magnetic resonance to examine the concentration change during the dip coating process

References

Abbott, J., Tetlow, N., Graham, A., Altobelli, S., Fukushima, E., Mondy, L., and Stephens, T. (1991). Experimental observations of particle migration in concentrated suspensions: Couette flow. *Journal of rheology, 35*(5), 773-795.

Abkarian, M., Nunes, J., and Stone, H. A. (2004). Colloidal crystallization and banding in a cylindrical geometry. *Journal of the American Chemical Society, 126*(19), 5978-5979.

Adachi, E., Dimitrov, A. S., and Nagayama, K. (1995). Stripe patterns formed on a glass surface during droplet evaporation. *Langmuir, 11*(4), 1057-1060.

Afanasiev, K., Münch, A., and Wagner, B. (2007). Landau-Levich problem for non-Newtonian liquids. *Physical Review E, 76*(3), 036307.

Amsden, A. A., Ruppel, H. M. and Hirt, C. W. (1980). A simplified ALE computer program for fluid flow at all speeds. *Los Alamos Scientific Laboratory Report*. LA-8095.

Asher, S. A., Alexeev, V. L., Goponenko, A. V., Sharma, A. C., Lednev, I. K., Wilcox, C. S., and Finegold, D. N. (2003). Photonic crystal carbohydrate sensors: low ionic strength sugar sensing. *Journal of the American Chemical Society, 125*(11), 3322-3329.

Aveyard, R., and Clint, J. H. (1996). Particle wettability and line tension. *Journal of the Chemical Society, Faraday Transactions, 92*(1), 85-89.

Bird, R., Stewart, W., and Lightfoot, E. (1960). Transport Phenomena, 780 pp: John Wiley, New York.

Blake, T., and Ruschak, K. (1979). A maximum speed of wetting. *Nature, 282*(5738), 489.

Borchers, K., Weber, A., Brunner, H., and Tovar, G. E. (2005). Microstructured layers of spherical biofunctional core-shell nanoparticles provide enlarged reactive surfaces for protein microarrays. *Analytical and bioanalytical chemistry, 383*(5), 738-746.

Brinker, C., Hurd, A., Schunk, P., Frye, G., and Ashley, C. (1992). Review of sol-gel thin film formation. *Journal of Non-Crystalline Solids, 147*, 424-436.

Brinker, C. J. (2013). Dip coating *Chemical Solution Deposition of Functional Oxide Thin Films* (pp. 233-261): Springer.

Burkert, K., Neumann, T., Wang, J., Jonas, U., Knoll, W., and Ottleben, H. (2007). Automated preparation method for colloidal crystal arrays of monodisperse and binary colloid mixtures by contact printing with a pintool plotter. *Langmuir, 23*(6), 3478-3484.

Cairncross, R. A., Schunk, P. R., Baer, T. A., Rao, R. R., and Sackinger, P. A. (2000). A finite element method for free surface flows of incompressible fluids in three dimensions. Part I. Boundary fitted mesh motion. *International journal for numerical methods in fluids, 33*(3), 375-403.

Campana, Valdez Silva, L., and Carvalho, M. (2017). Slot coating flows of non-colloidal particle suspensions. *AIChE Journal, 63*(3), 1122-1131.

Colosqui, C. E., Morris, J. F., and Stone, H. A. (2013). Hydrodynamically driven colloidal assembly in dip coating. *Physical review letters, 110*(18), 188302.

Cui, Y., Björk, M. T., Liddle, J. A., Sönnichsen, C., Boussert, B., and Alivisatos, A. P. (2004). Integration of colloidal nanocrystals into lithographically patterned devices. *Nano Letters, 4*(6), 1093-1098.

Denkov, N., Velev, O., Kralchevski, P., Ivanov, I., Yoshimura, H., and Nagayama, K. (1992). Mechanism of formation of two-dimensional crystals from latex particles on substrates. *Langmuir, 8*(12), 3183-3190.

Derjaguin, B. (1993). On the thickness of the liquid film adhering to the walls of a vessel after emptying. *Progress in Surface Science, 43*(1-4), 134-137.

Dimitrov, A. S., and Nagayama, K. (1996). Continuous convective assembling of fine particles into two-dimensional arrays on solid surfaces. *Langmuir, 12*(5), 1303-1311.

Donea, J. (1984). A Taylor–Galerkin method for convective transport problems. *International Journal for Numerical Methods in Engineering, 20*(1), 101-119.

Dushkin, C., Lazarov, G., Kotsev, S., Yoshimura, H., and Nagayama, K. (1999). Effect of growth conditions on the structure of two-dimensional latex crystals: experiment. *Colloid and Polymer Science, 277*(10), 914-930.

Fan, F., and Stebe, K. J. (2005). Size-selective deposition and sorting of lyophilic colloidal particles on surfaces of patterned wettability. *Langmuir, 21*(4), 1149-1152.

Fiegel, J., Jin, F., Hanes, J., and Stebe, K. (2005). Wetting of a particle in a thin film. *Journal of colloid and interface science, 291*(2), 507-514.

Gadala-Maria, F., and Acrivos, A. (1980). Shear-induced structure in a concentrated suspension of solid spheres. *Journal of rheology, 24*(6), 799-814.

Gadala-Maria, F. A., Andreas. (1980). Shear-induced structure in a concentrated suspension of solid spheres. *Journal of rheology, 24*(6), 799-814.

Ghosh, M., Fan, F., and Stebe, K. J. (2007). Spontaneous pattern formation by dip coating of colloidal suspensions on homogeneous surfaces. *Langmuir, 23*(4), 2180-2183.

Groenveld, P. (1971). Drainage and withdrawal of liquid films. *AIChE Journal, 17*(2), 489-490.

Hahn, R., and Seraphin, B. (1978). Spectrally selective surfaces for photothermal solar energy conversion. *Physics of thin films, 10*, 1-69.

Hayashi, S., Kumamoto, Y., Suzuki, T., and Hirai, T. (1991). Imaging by polystyrene latex particles. *Journal of colloid and interface science, 144*(2), 538-547.

Hinch. (2011). The measurement of suspension rheology,. *Journal of Fluid Mechanics*(686), 1-4.

Hoffman, R. L. (1972). Discontinuous and dilatant viscosity behaviour in concentrated suspensions. I. Observations of a flow instability. *Trans. Soc.Rheol, 16*, 155-173.

Holgado, M., Garcia-Santamaria, F., Blanco, A., Ibisate, M., Cintas, A., Miguez, H., Serna, C., Molpeceres, C., Requena, J., and Mifsud, A. (1999). Electrophoretic deposition to control artificial opal growth. *Langmuir, 15*(14), 4701-4704.

Holtz, J. H., and Asher, S. A. (1997). Polymerized colloidal crystal hydrogel films as intelligent chemical sensing materials. *Nature, 389*(6653), 829.

Huang, J., Kim, F., Tao, A. R., Connor, S., and Yang, P. (2005). Spontaneous formation of nanoparticle stripe patterns through dewetting. *Nature materials, 4*(12), 896.

Husband, D., Mondy, L., Ganani, E., and Graham, A. (1994). Direct measurements of shear-induced particle migration in suspensions of bimodal spheres. *Rheologica Acta, 33*(3), 185-192.

Javidi, M., and Hrymak, A. N. (2015). Numerical simulation of the dip-coating process with wall effects on the coating film thickness. *Journal of Coatings Technology and Research, 12*(5), 843-853.

Javidi, M., and Hrymak, A. N. (2016). Simulation of concentrated suspensions in free surface systems. *The Canadian Journal of Chemical Engineering, 94*(11), 2145-2152.

Jenny, M., and Souhar, M. (2009). Numerical simulation of a film coating flow at low capillary numbers. *Computers & Fluids, 38*(9), 1823-1832.

Jiang, P., Bertone, J., Hwang, K., and Colvin, V. (1999). Single-crystal colloidal multilayers of controlled thickness. *Chemistry of Materials, 11*(8), 2132-2140.

Joannopoulos, J. D., Villeneuve, P. R., and Fan, S. (1997). Photonic crystals: putting a new twist on light. *Nature, 386*(6621), 143.

Juillerat, F., Solak, H. H., Bowen, P., and Hofmann, H. (2005). Fabrication of large-area ordered arrays of nanoparticles on patterned substrates. *Nanotechnology, 16*(8), 1311.

Kheshgi, H., Kistler, S., and Scriven, L. (1992). Rising and falling film flows: viewed from a first-order approximation. *Chemical Engineering Science, 47*(3), 683-694.

Kim, O., and Nam, J. (2017). Confinement effects in dip coating. *Journal of Fluid Mechanics, 827*, 1-30.

Kralchevsky, P., and Nagayama, K. (2001). *Particles at fluid interfaces and membranes*: Elsevier Science Amsterdam.

Krechetnikov, R., and Homsy, G. (2005). Experimental study of substrate roughness and surfactant effects on the Landau-Levich law. *Physics of Fluids, 17*(10), 102108.

Krechetnikov, R., and Homsy, G. M. (2006). Surfactant effects in the Landau–Levich problem. *Journal of Fluid Mechanics, 559*, 429-450.

Krieger, I. M. (1963). A dimensional approach to colloid rheology. *Transactions of the Society of Rheology, 7*(1), 101-109.

Krieger, I. M. (1972). Rheology of monodisperse lattices. *Advances in Colloid and Interface Science, 3*, 111.

Landau., and Levich. (1942). Dragging of a liquid by a moving plate,. *Acta physicochem. URSS, 17*, 42.

Lee, C. Y., and Tallmadge, J. A. (1973). The stagnation point in free coating. *AIChE Journal, 19*(4), 865-866.

Lee, C. Y., and Tallmadge, J. A. (1975). Meniscus Shapes in Withdrawal of Flat Sheets from Liquid Baths. II. A Quasi-One-Dimensional Flow Model for Low Capillary Numbers. *Industrial & Engineering Chemistry Fundamentals, 14*(2), 120-126.

Leighton, D., and Acrivos, A. (1986). Viscous resuspension. *Chemical Engineering Science, 41*(6), 1377-1384.

Leighton, D., and Acrivos, A. (1987a). Measurement of shear-induced self-difusion in concentrated suspensions of spheres. *Journal of Fluid Mechanics*(177), 109-131.

Leighton, D., and Acrivos, A. (1987b). The shear-induced migration of particles in concentrated suspensions. *Journal of Fluid Mechanics, 181*, 415-439.

Li, J., Xing, R., Huang, W., and Han, Y. (2005). A self-assembly approach to fabricate the patterned colloidal crystals with a tunable structure. *Colloids and Surfaces A: Physicochemical and Engineering Aspects, 269*(1-3), 22-27.

Lyon, M., and Leal, L. (1998). An experimental study of the motion of concentrated suspensions in two-dimensional channel flow. Part 1. Monodisperse systems. *Journal of Fluid Mechanics, 363*, 25-56.

Marques, D., Costanza, V., and Cerro, R. L. (1978). Dip coating at large capillary numbers: An initial value problem. *Chemical Engineering Science, 33*(1), 87-93.

Mewis, J., and Wagner, N. J. (2012). *Colloidal suspension rheology*: Cambridge University Press.

Middleman, S. (1977). *Fundamentals of polymer processing*: McGraw-Hill New York.

Min, K. H., and Kim, C. (2010). Simulation of particle migration in free-surface flows. *AIChE Journal, 56*(10), 2539-2550.

Mukhopadhyay, S., Usha, R., and Tulapurkara, E. (2009). Numerical study of concentrated fluid–particle suspension flow in a wavy channel. *International journal for numerical methods in fluids, 59*(10), 1125-1155.

Nguyen, V. X., and Stebe, K. J. (2002). Patterning of small particles by a surfactant-enhanced Marangoni-Bénard instability. *Physical review letters, 88*(16), 164501.

Park, C.-W., and Homsy, G. (1984). Two-phase displacement in Hele Shaw cells: theory. *Journal of Fluid Mechanics, 139*, 291-308.

Park, S. H., and Xia, Y. (1998). Macroporous membranes with highly ordered and three-dimensionally interconnected spherical pores. *Advanced Materials, 10*(13), 1045-1048.

Peralta, J. M., Meza, B. r. E., and Zorrilla, S. E. (2014). Mathematical modeling of a dip-coating process using a generalized Newtonian fluid. 1. Model development. *Industrial & Engineering Chemistry Research, 53*(15), 6521-6532.

Phillips, R. J., Armstrong, R. C., Brown, R. A., Graham, A. L., and Abbott, J. R. (1992). A constitutive equation for concentrated suspensions that accounts for shear-induced particle migration. *Physics of Fluids A: Fluid Dynamics, 4*(1), 30-40.

Quéré, D. (1999). Fluid coating on a fiber. *Annual Review of Fluid Mechanics, 31*(1), 347-384.

Rao, R., Mondy, L., Sun, A., and Altobelli, S. (2002). A numerical and experimental study of batch sedimentation and viscous resuspension. *International journal for numerical methods in fluids, 39*(6), 465-483.

Ray, M. A., Kim, H., and Jia, L. (2005). Dynamic self-assembly of polymer colloids to form linear patterns. *Langmuir, 21*(11), 4786-4789.

Rebouças, R., Siqueira, I., and Carvalho, M. (2018). Slot coating flow of particle suspensions: Particle migration in shear sensitive liquids. *Journal of non-newtonian fluid mechanics, 258*, 22-31.

Ritz, J.-B., Bertrand, F., Thibault, F., and Tanguy, P. (2000). Shear-induced particle migration in a short-dwell coater. *Chemical Engineering Science, 55*(21), 4857-4867.

Roy, S., and Dutt, D. (1981). Wire coating by withdrawal from a bath of power law fluid. *Chemical Engineering Science, 36*(12), 1933-1939.

Ryck, A., and Quéré, D. (1996). Inertial coating of a fibre. *Journal of Fluid Mechanics, 311*, 219-237.

Sackinger, P. A., Schunk, P. R., and Rao, R. R. (1996). A Newton–Raphson pseudo-solid domain mapping technique for free and moving boundary problems: a finite element implementation. *Journal of Computational Physics, 125*(1), 83-103.

Sartor, L., and Scriven, L. (1990). *The progression from dip coating to slot coating: what controls film thickness.* Paper presented at the AIChE Annual Meeting.

Schunk, P., Sackinger, P., and Rao, R. (1996). GOMA-A full-Newton finite element program for free and moving boundary problems with coupled fluid/solid momentum, energy, mass, and chemical species transport: Users guide: Sandia National Labs., Albuquerque, NM (United States).

Schunk, P. R., Rao, R. R., Chen, K. S., Labreche, D. A., Sun, A. C.-T., Hopkins, M. M., Moffat, H. K., Roach, R. A., Hopkins, P. L., and Notz, P. K. (2013). GOMA 6.0: Sandia National Laboratories (SNL-NM), Albuquerque, NM (United States); 3M Company,, St. Paul, MN.

Schunk, R., Hurd, A. J., and Brinker, C. J. (1997). Free-meniscus coating processes *Liquid film coating* (pp. 673-708): Springer.

Scriven, L. (1988). Physics and applications of dip coating and spin coating. *MRS Online Proceedings Library Archive, 121*.

Stephan F. Kistler, K. N. C., P. Randall Schunk. (1997). *Liquid Film Coating: Scientific principles and their technological implications*: Chapman & Hall, London.

Stickel, P. (2005). Fluid mechanics and rheology of dense suspensions. *Annual Review of Fluid Mechanics*(37), 129-149.

Sun, C.-H., Linn, N. C., and Jiang, P. (2007). Templated fabrication of periodic metallic nanopyramid arrays. *Chemistry of Materials, 19*(18), 4551-4556.

Tadros, T. F. (2011). *Rheology of dispersions: principles and applications*: John Wiley & Sons.

Tanguy, P., Fortin, M., and Choplin, L. (1984). Finite element simulation of dip coating, II: Non-Newtonian fluids. *International journal for numerical methods in fluids, 4*(5), 459-475.

Tetlow, N., Graham, A. L., Ingber, M. S., Subia, S. R., Mondy, L. A., and Altobelli, S. A. (1998). Particle migration in a Couette apparatus: experiment and modeling. *Journal of rheology, 42*(2), 307-327.

Velev, O., Jede, T., Lobo, R., and Lenhoff, A. (1997). Porous silica via colloidal crystallization. *Nature, 389*(6650), 447.

Watanabe, S., Inukai, K., Mizuta, S., and Miyahara, M. T. (2009). Mechanism for stripe pattern formation on hydrophilic surfaces by using convective self-assembly. *Langmuir, 25*(13), 7287-7295.

White, D., and Tallmadge, J. (1965). Theory of drag out of liquids on flat plates. *Chemical Engineering Science, 20*(1), 33-37.

White, D. A., and Tallmadge, J. A. (1966). A theory of withdrawal of cylinders from liquid baths. *AIChE Journal, 12*(2), 333-339.

Yin, Y., Lu, Y., Gates, B., and Xia, Y. (2001). Template-assisted self-assembly: a practical route to complex aggregates of monodispersed colloids with well-defined sizes, shapes, and structures. *Journal of the American Chemical Society, 123*(36), 8718-8729.

Zhang, K., and Acrivos, A. (1994). Viscous resuspension in fully developed laminar pipe flows. *International journal of multiphase flow, 20*(3), 579-591.

Zheng, H., Lee, I., Rubner, M. F., and Hammond, P. T. (2002). Two component particle arrays on patterned polyelectrolyte multilayer templates. *Advanced Materials, 14*(8), 569-572.

Appendices

Experimental

Polystyrene particles and food grade mineral oil (FG WO35, Petro Canada) were chosen in order to study the effect of bath width on the deposition of particles in the final film. High resolution and high-speed camera (IO industries camera model Flare 4M180-Cl – resolution 2048× 20148 pixel) captured the image of the substrate surface. The camera was fixed at a suitable distance while it was perpendicular to the substrate. Sufficient light was projected during the image taking. Images were recaptured three times for each bath size.

Dip coating apparatus has been used for immersing process of the substrate into the suspension fluid at a constant velocity by vertical withdrawal (Figure 32).

The cylindrical substrate with a radius of 1590 µm has selected to be the large size for capturing the images clearly. The ratio of bath radius to the substrate radius (R/r) was considered the variable parameter at this study with four different bath sizes with the ratio of $R/r = 4,8,12,16$ were tested. The substrate velocity fixed at 5 cm/s and the initial concentration of suspension was 0.1 vol%.
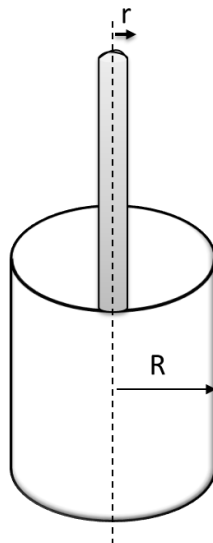
Figure 32 : (R) is the bath radius and (r) is the cylinder substrate radius

In this study, MATLAB® R2018b was used to accomplish the image processing. MATLAB algorithm helps detect the area covered with the polystyrene particles scattered on the surface of the substrate. The total area of the substrate surface which is covered by polystyrene particles was calculated.
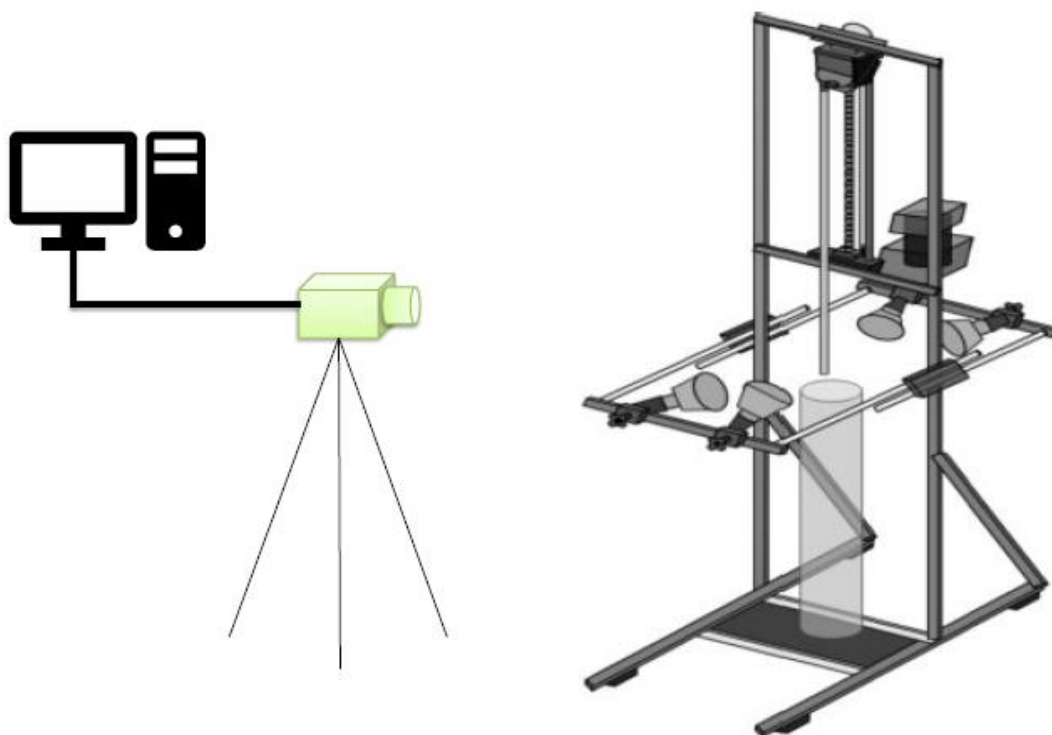
Figure 33: Dip coating apparatus along with the camera

For suspensions prepared with a Newtonian carrier fluid, mineral oil, and polystyrene particles the experimental investigations have been carried out. The area which is detected and visualized by deposited particles was selected as the quantifiable parameter for this examination. An image analysis algorithm is applied to detect spherical particles. In all measurement, the velocity is 5 cm/s and with 20% suspension concentration.

Figure 34 shows the results of the covered area by polystyrene particles on the surface in different bath radius. By increasing the ratio of the bath radius, the total particle distribution area on the substrate surface is increased. It should be noted that all surfaces were well coated by oil and difference rises in the particle deposition.

Based on the simulation and experimental results, the smaller bath is exposed to a higher shear rate affected by the wall proximity; hence, leading to deposition of fewer particles on the substrate surface.

The knowledge of the coating bath characteristics would have supported the advancement of the final film structure.
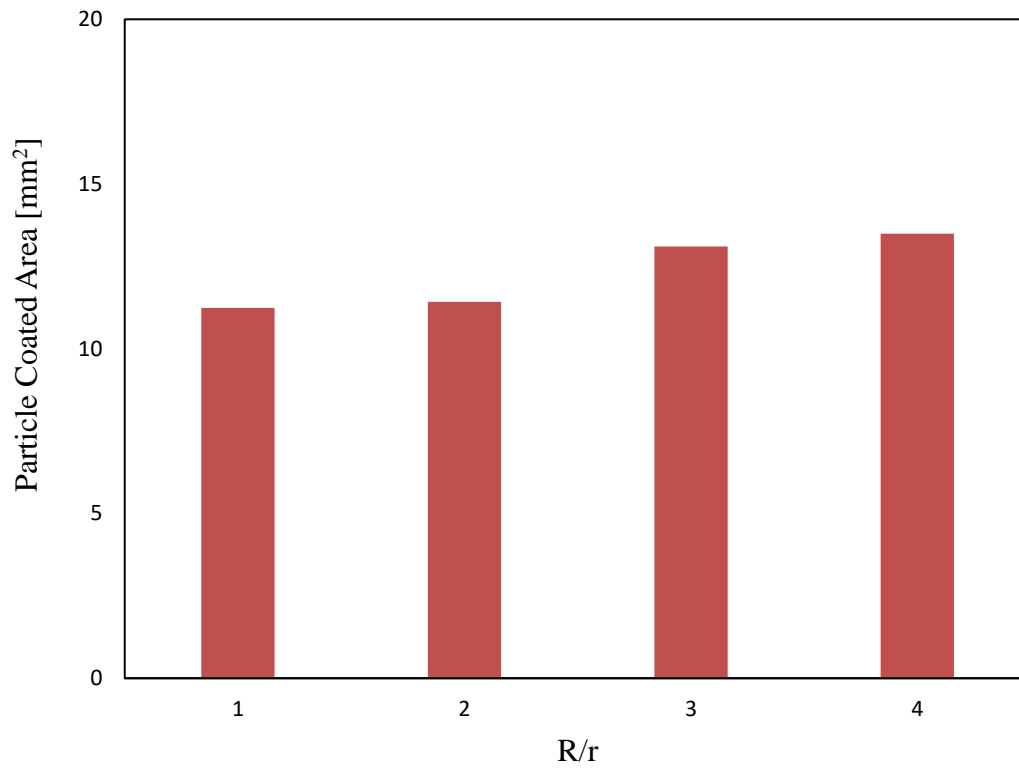

Figure 34: Experimental results of the area covered with particles on the substrate surface in different bath size

Figure 35 depicted the captured images of a substrate at the different bath radius. The white spots represent the polystyrene particles deposited on the surface.
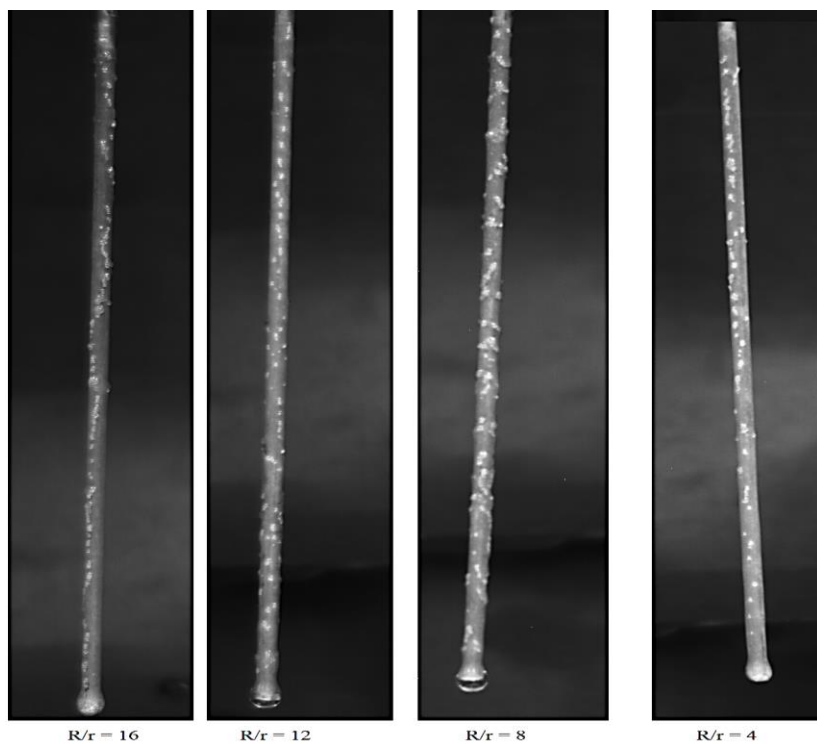

R/r = 16   R/r = 12   R/r = 8   R/r = 4

Figure 35: Captured images of a cylindrical substrate in different bath geometry

Curriculum Vitae

Name: Mahdieh Moghadasi

Post-secondary Education and Degrees: Arak University
Arak, Iran
2008-2012 B.A.

The University of Western Ontario
London, Ontario, Canada
2016-2019 MESc.

Related Work Experience   Teaching Assistant, Fluid Flow
The University of Western Ontario
2017

Publications:

M. Garmsiri, H. R. Mortaheb, **M. Moghadasi**, "High performance nanocomposite cation exchange membrane: Effects of functionalized silica-coated magnetic nanoparticles" Journal of Membrane Science and Research, 2017

M. Garmsiri, H. R. Mortaheb, **M. Moghadasi**, "Effects of functionalized silica nanoparticles on characteristics of nanocomposite sPES cation exchange membranes", journal of Wuhan University of Technology, 2017

M. Moghadasi, H. R. Mortaheb, "Incorporating functionalized silica nanoparticles in polyethersulfone-based anion exchange nanocomposite membranes", Journal of Applied Polymer Science, 2017, 134 (11)

M. J. Moghadasi, I. Lotfi, **M. Moghadasi**, "Comparison of Correlations for Predicting Oil Flow Rate Passing through Chokes", Energy Source Part A, 2015, 12, 1340-1345.